Title
Observation-based modeling of ozone chemistry in the Seoul metropolitan area during the Korea-United States Air Quality Study (KORUS-AQ)

Journal
Elementa, 8(1)

ISSN
2785-4558

Authors
Schroeder, JR
Crawford, JH
Ahn, JY
et al.

Publication Date
2020

DOI
10.1525/elementa.400

ELEMENTA
Science of the Anthropocene

Schroeder, JR, et al. 2020. Observation-based modeling of ozone chemistry in the Seoul metropolitan area during the Korea-United States Air Quality Study (KORUS-AQ). *Elem Sci Anth,* 8: 3. DOI: https://doi.org/10.1525/elementa.400

RESEARCH ARTICLE

Observation-based modeling of ozone chemistry in the Seoul metropolitan area during the Korea-United States Air Quality Study (KORUS-AQ)

Jason R. Schroeder[*,†], James H. Crawford[*], Joon-Young Ahn[‡], Limseok Chang[‡], Alan Fried[§], James Walega[§], Andrew Weinheimer[‖], Denise D. Montzka[‖], Samuel R. Hall[‖], Kirk Ullmann[‖], Armin Wisthaler[¶,**], Tomas Mikoviny[¶], Gao Chen[*], Donald R. Blake[††], Nicola J. Blake[††], Stacey C. Hughes[††], Simone Meinardi[††], Glenn Diskin[*], Joshua P. Digangi[*], Yonghoon Choi[*], Sally E. Pusede[‡‡], Greg L. Huey[§§], David J. Tanner[§§], Michelle Kim[‖‖] and Paul Wennberg[‖‖]

The Seoul Metropolitan Area (SMA) has a population of 24 million and frequently experiences unhealthy levels of ozone (O_3). In this work, measurements taken during the Korea-United States Air Quality Study (KORUS-AQ, 2016) are used to explore regional gradients in O_3 and its chemical precursors, and an observationally-constrained 0-D photochemical box model is used to quantify key aspects of O_3 production including its sensitivity to precursor gases. Box model performance was evaluated by comparing modeled concentrations of select secondary species to airborne measurements. These comparisons indicate that the steady state assumption used in 0-D box models cannot describe select intermediate species, highlighting the importance of having a broad suite of trace gases as model constraints. When fully constrained, aggregated statistics of modeled O_3 production rates agreed with observed changes in O_3, indicating that the box model was able to represent the majority of O_3 chemistry.

Comparison of airborne observations between urban Seoul and a downwind receptor site reveal a positive gradient in O_3 coinciding with a negative gradient in NO_x, no gradient in CH_2O, and a slight positive gradient in modeled rates of O_3 production. Together, these observations indicate a radical-limited (VOC-limited) O_3 production environment in the SMA. Zero-out simulations identified C_{7+} aromatics as the dominant VOC contributors to O_3 production, with isoprene and anthropogenic alkenes making smaller but appreciable contributions. Simulations of model sensitivity to decreases in NO_x produced results that were not spatially uniform, with large increases in O_3 production predicted for urban Seoul and decreases in O_3 production predicted for far-outlying areas. The policy implications of this work are clear: Effective O_3 mitigation strategies in the SMA must focus on reducing local emissions of C_{7+} aromatics, while reductions in NO_x emissions may increase O_3 in some areas but generally decrease the regional extent of O_3 exposure.

Keywords: Ozone; Air quality; Photochemistry; Korea; Seoul

1. Introduction

Rapid industrial growth and urban expansion in South Korea over the past several decades has been accompanied by increased exposure to criteria pollutants such as ozone (O_3), particularly in the Seoul Metropolitan Area (SMA) (Jo and Nam, 1999; Ghim and Chang, 2000; Chang et al., 2017; Kim and Lee, 2018; Seo et al., 2018; Fleming et al., 2018). Exposure to high levels of O_3 is deleterious to

* NASA Langley Research Center, Hampton, VA, US
† NASA Postdoctoral Program, NASA Langley Research Center, Hampton, VA, US
‡ National Institute of Environmental Research, Incheon, KR
§ Institute of Arctic and Alpine Research, University of Colorado, Boulder, CO, US
‖ National Center for Atmospheric Research, Boulder, CO, US
¶ Institute for Ion Physics and Applied Physics, University of Innsbruck, AT
** Department of Chemistry, University of Oslo, Oslo, NO
†† Department of Chemistry, University of California Irvine, Irvine, CA, US
‡‡ Department of Environmental Sciences, University of Virginia, Charlottesville, VA, US
§§ School of Earth and Atmospheric Sciences, Georgia Institute of Technology, Atlanta, Georgia, US
‖‖ Division of Engineering and Applied Sciences, California Institute of Technology, Pasadena, California, US
Corresponding author: Jason R. Schroeder (schroede.jaso@gmail.com)

human health and the environment, and has been linked to increased human mortality and decreased crop yields (Haagen-Smit et al., 1952; Heck et al., 1982; Chameides et al., 1999; Kim et al., 2004; Jerrett et al., 2009). Fleming et al. (2018) noted that the annual fourth-highest maximum daily 8-hour average (MDA8) O_3 value increased at an average rate of 2 ppbv per year between 2000–2014, and the number of days with 8-hour O_3 values greater than 70 ppbv increased by up to two days per year across South Korea. While ambient O_3 levels in South Korea have been increasing for some time, recent work by Jung et al. (2018) suggests that the rate of increase has risen in recent years. Broader analysis of trends across greater East Asia has shown that O_3 values throughout the region have been increasing in the past decade, raising questions about the influence of regional versus local emissions on air quality in the SMA (Chang et al., 2017). However, the trends noted by Fleming et al. (2018) and Chang et al. (2017) were significantly more prevalent at urban sites in South Korea than at rural sites, indicating that, while long-range transport may contribute to increasing background levels of O_3, local emissions must be addressed in order to improve air quality. In this work, data collected during the Korea United States Air Quality Study (KORUS-AQ) are used to better understand the primary drivers for O_3 in the SMA.

There are no primary emission sources of O_3, and instead it is formed through the photochemical interaction between emissions of volatile organic compounds (VOCs) and nitrogen oxides ($NO_x = NO + NO_2$). Therefore, strategies to reduce O_3 in the SMA must focus on reducing local and regional emissions of these precursor species. However, O_3 chemistry is complex and varies non-linearly with respect to precursor concentrations, and therefore a detailed understanding of the sensitivity of local O_3 formation to changes in the precursor environment is essential for drafting effective mitigation strategies. This non-linear response of O_3 to concentrations of its precursors results in the presence of two distinct photochemical regimes, often referred to as "NO_x-limited" and "radical-limited" (also called "VOC-limited" due to the relationship between VOCs and radicals) (Sillman et al., 1990; Kleinman, 1994). Understanding local O_3 sensitivity (i.e. whether O_3 formation is NO_x-limited or radical-limited) is a crucial first step for drafting targeted mitigation strategies. Formation of O_3 in the background troposphere is typically NO_x-limited, while the urban areas around many megacities are often radical-limited (Duncan et al., 2010). However, these terms should not be taken to imply either/or solutions for ozone mitigation. For instance, megacities are not radical-limited because of minimal VOC emissions, but rather because of an overabundance of NO_x, making the term "NO_x-saturated" a more appropriate term. In such "NO_x-saturated" environments, reduction of NO_x is necessary to achieve long-term ozone reduction but would be expected to lead to short-term ozone increases without concurrent action to reduce VOC emissions. In this work, the terms "radical-limited", "VOC-limited", and "NO_x-saturated" are taken to have the same meaning, and we choose to use "radical-limited" for simplicity.

While classifying regional O_3 production as NO_x-limited or radical-limited is an important first step, we must note that "VOCs" refers to a collection of hundreds of distinct trace gases arising from a variety of anthropogenic and natural sources, each with unique rates of reaction with OH and unique radical yields upon oxidation. Therefore, in radical-limited (i.e. VOC-limited) environments, investigating the sensitivity of O_3 to individual VOCs or subsets of similar VOCs is necessary for developing mitigation strategies that target emissions sectors that contribute disproportionately to local O_3 formation.

Effective O_3 control strategies rely on accurate understanding of how ambient O_3 levels would respond to reductions in precursor emissions; thus, potential biases or uncertainties from model-based and observation-based studies must be taken into consideration. 3D models that include emissions, transport, and chemistry are well-suited for exploring the response of simulated O_3 to reductions in modeled emissions, but are subject to large uncertainties in many parameters (particularly emissions) that lead to uncertainties in simulated O_3 and the simulated dependence of O_3 on its precursors (Sillman, 1995, 2003; Sillman et al., 1998; Zhou et al., 2013; Choi and Souri, 2015; Goldberg et al., 2016). Ground-based studies that make use of O_3 sensitivity indicators (as described in Sillman and He (2002) and Schroeder et al. (2017)) have the advantage of making direct observations of the real atmosphere, but may be limited to one location, making it difficult to understand how representative they are of a broader region (Thornton et al., 2002; Mao et al., 2010; Edwards et al., 2013; Ren et al., 2013). Furthermore, recent work has highlighted the presence of vertical gradients in O_3 precursors within the boundary layer, suggesting that significant bias can arise if surface observations are used to infer integrated rates of O_3 production throughout the boundary layer (Zhang et al., 2016). Airborne studies, on the other hand, provide measurements of O_3 and its precursors over large geographical areas, allowing for calculation of O_3 production rates and O_3 sensitivity at local and regional scales across vertical gradients (Kleinman et al., 2001, 2002; Mazzuca et al., 2016; Schroeder et al., 2017). This work uses data collected onboard the NASA DC-8 aircraft during the Korea-United States Air Quality Study (KORUS-AQ; May 2–June 11, 2016) to explore gradients in O_3 and its chemical precursors in the SMA, and uses an observationally-constrained box model to quantify the response of simulated O_3 production rates to perturbations in the precursor environment. While much can be learned from analysis of box model calculations, care must be taken to ensure that the constraints used to drive the model and the underlying chemical mechanism within the model adequately represent conditions in the SMA. For this reason, a large portion of this work (Section 4) is dedicated to analysis of model performance against a number of metrics, including comparison of model-calculated abundances of secondary "test species" to observations, and comparison of calculated rates of O_3 production to observed changes in O_3.

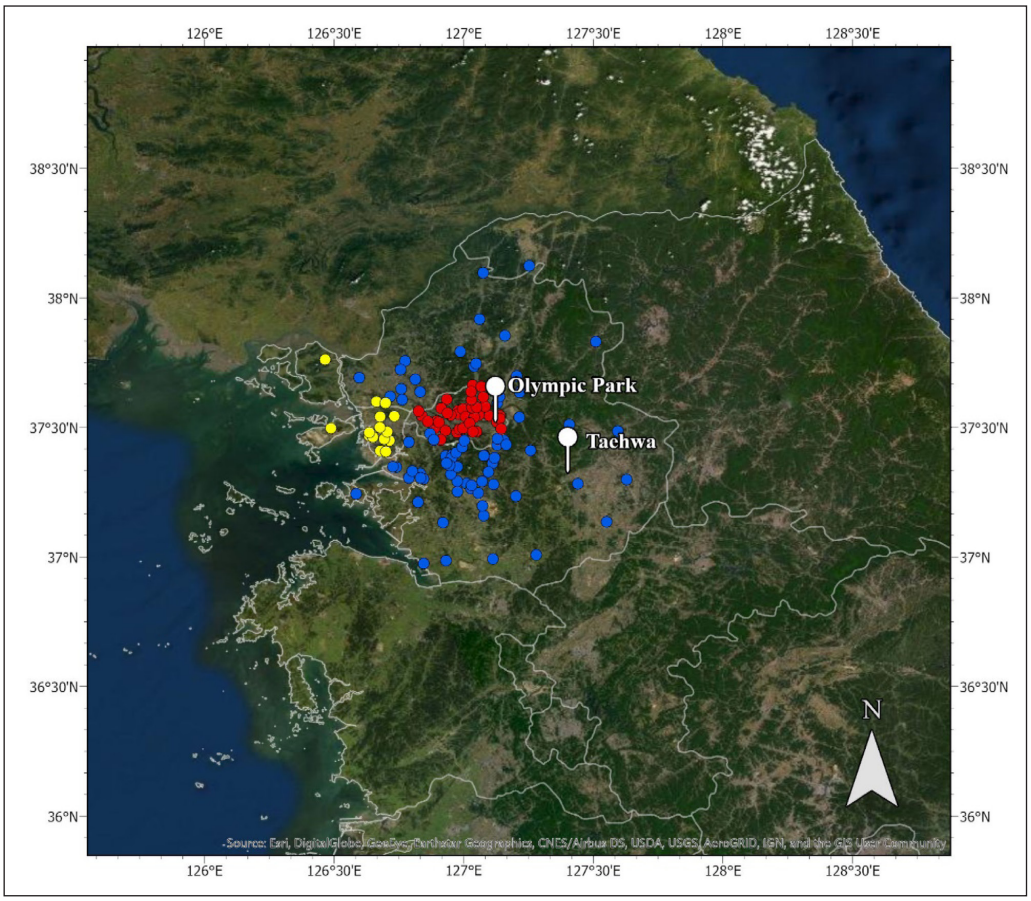

Figure 1: Map of O_3 monitors in the SMA, with pins showing the locations of Olympic Park and Taehwa Forest, two key sites that will be discussed in greater detail in Section 3. O_3 monitors are colored by subregion within the SMA: Urban Seoul (red), Incheon (yellow), and Gyeonggi (blue). DOI: https://doi.org/10.1525/elementa.400.f1

2. Distribution of surface O_3 in the SMA during KORUS-AQ

To help place the KORUS-AQ observations into context, it is useful to first examine the distribution of surface ozone observed by the AirKorea network of air quality monitoring sites. KORUS-AQ was conducted during the climatological peak of O_3 season in South Korea that occurs during the pre-monsoon period in late spring/early summer, typically during May and June (Ghim and Chang, 2000; Jo et al., 2000; Kim et al., 2006). Therefore, the timing of the field deployment is germane to exploring spatiotemporal tendencies in O_3 and conducting policy-relevant analysis of the key drivers of O_3 formation.

The SMA has a population of approximately 25 million, divided into three main regions: Urban Seoul (population 10 million), the Incheon metropolitan city (population 3 million), and the surrounding Gyeonggi province (population 12 million). **Figure 1** shows the location of air quality monitoring sites maintained in these three regions by the National Institute of Environmental Research (NIER) as part of the larger country-wide AirKorea network. Statistics for observations across these sites are summarized in **Table 1**. Percentile statistics for sites across the three regions are provided for MDA8 O_3, associated levels of O_x (O_3 + NO_2), and number of exceedance days in each region. Exposure to high O_3 levels is significantly greater for sites in Gyeonggi province with monitors recording MDA8 O_3 values in excess of the Korean standard of 60 ppbv roughly half of the time. Seoul and Incheon experience such values, but only violate the Korean standard a little over a quarter of the time with lower O_3 values that tend to be about 10 ppbv less than those observed in Gyeonggi province. This difference can be better understood when looking at statistics for the associated O_x values, which show Seoul to have values that run a few ppbv higher than Gyeonggi due to the proximity to greater NO_x emissions. While Incheon values of O_x are still lower than Gyeonggi, the regional difference in O_x is smaller than that for O_3. Based on these statistics, the greater number of exceedance days for Gyeonggi province can be attributed mainly to the lower NO_x levels in comparison to Seoul and Incheon rather than higher overall oxidant levels. These observations drive the motivation for this work, which broadly aims to answer the following two questions: 1) Which O_3 precursor species are the primary drivers of O_3 production in the SMA? And 2) What mitigation strategies would be most effective for achieving reductions in O_3 across the SMA? This work uses measurements made onboard the NASA DC-8 aircraft during KORUS-AQ and observation-based modeling to explore these questions and provide policy-relevant information about the local photochemical environment.

Table 1: Percentile statistics for maximum daily average 8-hour (MDA8) O_3, MDA8 O_x, and the number of days with at least one monitor in exceedance (MDA8 O_3 > 60 ppbv) for AirKorea monitors in Seoul, Incheon, and Gyeonggi provinces during the KORUS-AQ study period, May 2–June 11, 2016. DOI: https://doi.org/10.1525/elementa.400.t1

Location (color in Fig. 1)	Urban Seoul (red)	Incheon (yellow)	Gyeonggi (blue)
Percentile Statistics for MDA8 O_3 at AirKorea monitors (units: ppbv)			
95th	82.0	83.0	90.6
75th	62.5	63.6	72.6
Median	49.5	50.9	60.0
25th	36.3	41.5	48.7
5th	21.1	29.5	35.5
Percentile Statistics for MDA8 O_x (O_3 + NO_2) at AirKorea monitors (units: ppbv)			
95th	120.7	110.3	115.8
75th	99.3	87.5	95.9
Median	83.8	73.3	80.0
25th	69.4	61.8	66.7
5th	53.6	48.0	52.7
Number of Exceedance Days (at least one monitor with MDA8 O_3 > 60 ppbv)			
# Days	33	26	39

3. Methods

3.1. KORUS-AQ Observations

KORUS-AQ was a multi-agency, multi-platform international field campaign that took place in South Korea from May 2–June 11, 2016. As part of KORUS-AQ, the NASA DC-8 aircraft performed 20 local research flights over South Korea. A map showing all local DC-8 flights during KORUS-AQ is shown in the top panel of **Figure 2**. During most research flights, the DC-8 flew a standard route over the SMA that was repeated during the morning (~9:00 local time), midday (~12:30 local time), and afternoon (~3:30 local time). This route is shown in the bottom panel of **Figure 2**, which descends over the city and passes over two instrumented supersites. The descent over the city began from ~2.5 km at the northern end of urban Seoul, passing over the Olympic Park site at ~0.5 km before coming within meters of the surface over the runway of Seoul Air Base, located about 8 km south of Olympic Park. From Seoul AB, the DC-8 proceeded at low altitude to pass over the Taehwa Forest research site at ~0.3 km before performing a wide ascending spiral up to ~10 km in the area to the east of Taehwa. Sampling along this route was performed on fifty-five occasions under a wide variety of air quality conditions. This provides a strong statistical basis for exploring the spatial and temporal variability over short term time scales (i.e. diurnal variability within one day) and relatively long time scales (i.e. day-to-day variability over the study period). The primary objective of KORUS-AQ was to collect measurements that would facilitate a better understanding of the chemical and physical processes that control air quality over South Korea, with an emphasis on collecting observations that could improve satellite-based remote sensing of air pollution. Because of this, the majority of flights during KORUS-AQ were conducted during sunny or partly cloudy conditions, which are also conducive to O_3 formation. Much of the KORUS-AQ study period was characterized by consistent high pressure with relatively weak synoptic flow. Under these conditions, characterized by stagnant airmasses in the morning and a building westerly sea breeze through the afternoon, Taehwa forest acted as a receptor site for outflow from urban Seoul.

The instrument payload of the DC-8 was designed to allow for detailed studies of gas phase and condensed phase chemical processes. The subset of airborne measurements that are directly related to this work include trace gases (O_3, NO, NO_2, CO, water vapor, CH_2O, PAN, H_2O_2, HNO_3, and speciated VOCs), meteorological variables, and photolysis rates. All DC-8 measurements used in this work are summarized in **Table 2**.

3.2. Box model setup

The observationally-constrained NASA Langley Research Center (LaRC) 0-D time-dependent photochemical box model was used to simulate ozone photochemistry during KORUS-AQ. The model was constrained by coincident observations of trace gases such as O_3, NO, CO, CH_4, CH_2O, water vapor, and non-methane hydrocarbons; by meteorological parameters such as temperature and pressure; and by photolysis rates derived from actinic flux observations. The model calculates the diurnal steady-state profiles of radicals and other computed species for each set of measurements along the flight path (Crawford et al., 1999; Olson et al., 2001, 2006). In effect, the model is integrated forward in time until all calculated species exhibit a reproducible diurnal cycle (i.e. convergence is met for each calculated species). Values are extracted for the specific time of the flight measurement to enable the calculation of instantaneous ozone production rates associated with the measurements along the flight path. During the simulated diurnal cycle, all constraining species are held constant. NO_x requires special treatment to allow interconversion between NO, NO_2 and other short-lived reactive nitrogen species during the diurnal cycle. In this case, the total abundance of NO_x is held constant but calculated to be consistent with the observed NO mixing ratio at the time of the measurement. The diurnal variation of photolysis frequencies is calculated for clear-sky conditions and scaled by the ratio of observed-to-clear-sky values at the time of the measurement. The most recent update to the chemical mechanism, including a complete list of all reactions used in the model is provided in Schroeder et al. (2017); however, updates to the aromatic chemistry mechanism have been made and are described later in this section.

In highly polluted conditions, the appropriateness of the steady-state assumption becomes less valid. For instance, Fried et al. (2011) demonstrated that model estimates of CH_2O can be biased in pollution plumes when short-lived

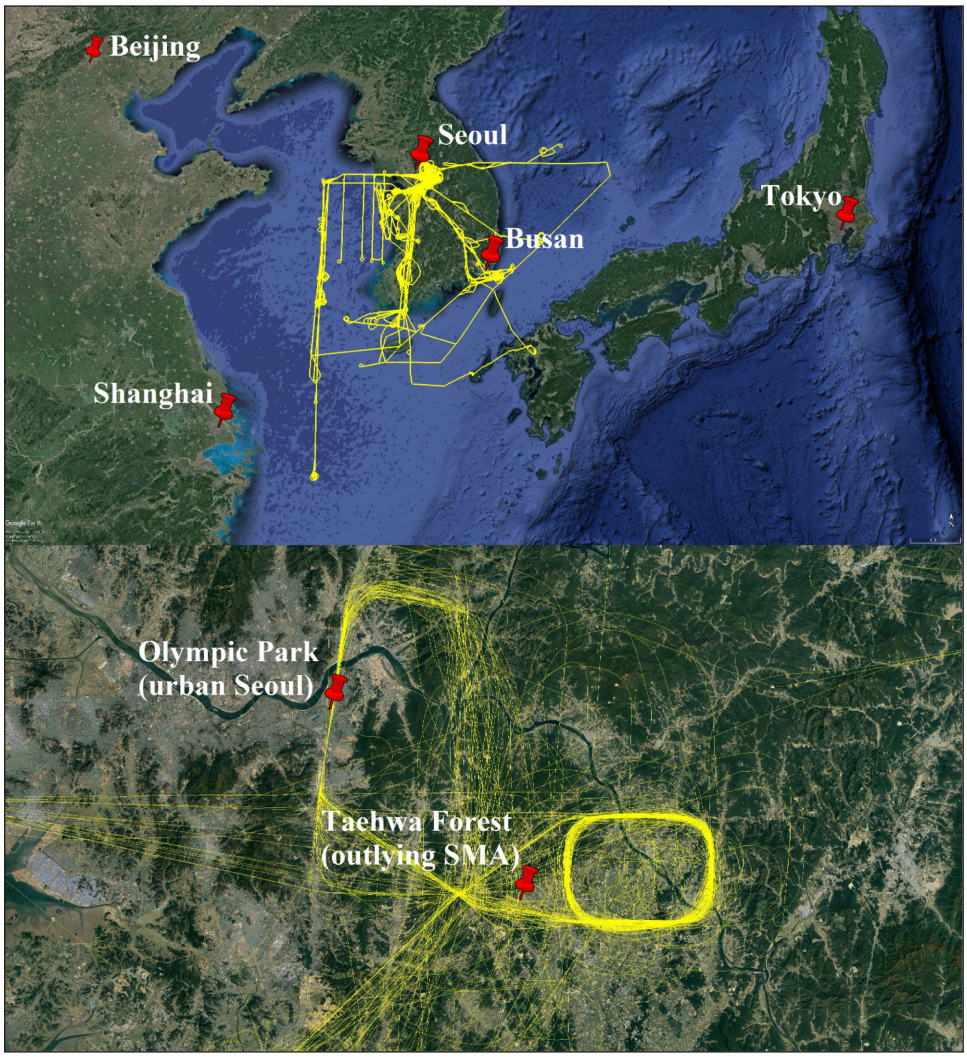

Figure 2: Maps of all DC-8 flights in the broader context of East Asia (top panel), and the repeated stereo route over the SMA (bottom panel). DOI: https://doi.org/10.1525/elementa.400.f2

Table 2: Summary of DC-8 measurements used in this work. DOI: https://doi.org/10.1525/elementa.400.t2

Instrument Name	Species Measured	Reference(s)
Diode Laser Hygrometer (DLH)	water vapor	(Diskin et al., 2002)
Differential Absorption CO Measuerment (DACOM)	CO, CH_4	(Sachse et al., 1991)
$NO_{xy}O_3$ Chemiluminescence	O_3, NO, NO_2	(Weinheimer et al., 1994)
Compact Atmospheric Multi-species Spectrometer (CAMS)	CH_2O, C_2H_6	(Weibring et al., 2010; Richter et al., 2015)
Proton Transfer Time of Flight Mass Spectrometer (PTR-TOF-MS)	methanol, acetone + propanal, isoprene, MVK + MACR, benzene, toluene, C_8 aromatics	(Muller et al., 2014)
Whole Air Sampler (WAS)[a]	C_2-C_{10} alkanes, C_2-C_4 alkenes, C_6-C_9 aromatics, isoprene	(Colman et al., 2001)
Georgia Tech Chemical Ionization Mass Spectrometer (GTCIMS)	PAN	(Slusher et al., 2004)
California Institute of Technology Chemical Ionization Mass Spectrometer (CIT-TOF-CIMS)	H_2O_2, CH_3OOH	(Crounse et al., 2006)
CCD-Based Actinic Flux Spectrometers (CAFS)	4π sr actinic flux and derived photolysis frequencies	(Shetter et al., 1999)

[a] All measurements taken at a minimum frequency of 1 Hz except WAS. WAS sample frequency ranged from every 0.5–5 min, depending on aircraft location relative to points of interest, with each canister requiring 0.5 to 1.5 min to fill. On a typical 8 hour flight, about 170 whole air samples were collected.

species dominate the model photochemistry, e.g., highly-reactive VOCs such as biogenic isoprene or alkenes from industrial sources. Under such conditions, using observations to constrain CH_2O and other important radical reservoirs instead of calculating them will improve model calculations of the radical pool responsible for ozone production. The intricacies of the steady-state assumption will be explored further in Section 4 using comparisons of fully-constrained and minimally-constrained model runs. Additional model uncertainties arise from uncertainties in measured constraints and uncertainties in kinetic and photolytic rates.

Model inputs for each flight were derived from DC-8 1-s merges (available at https://www-air.larc.nasa.gov/missions/korus-aq/index.html). However, creating 1-s model inputs from these DC-8 1-s merges involved many steps to maximize the number of data points that could be run by the model. At a minimum, The LaRC 0-D photochemical box model must be constrained by coincident measurements of CH_4, CO, NO, O_3, H_2O, and photolysis rates. To maximize the number of points that could be run by our model, an iterative median smoothing process was performed to fill in missing data points for these species. Missing data were replaced with the median of the surrounding ±3n data points, where n = 1, 2, 3, 4. In effect, this allows for the smallest smoothing window possible to be used for each missing value. First, we attempted to replace missing values with the median of the surrounding ±3 data points (i.e. n = 1), under condition that at least half of the data points within the window were not missing themselves. If that condition was not met, median smoothing was attempted with a window of the surrounding ±6 data points (i.e. n = 2), onwards until a final smoothing window of ± 12 data points (i.e. n = 4) was reached. Flying at an altitude of 1 km, the DC-8 would travel a distance of about 3 km in 24 seconds (i.e. the time duration of the maximum smoothing window, n = 4), and a maximum vertical distance of about 120 meters (the DC-8 typically ascended/descended at a maximum rate of 5 m/s). For the subset of KORUS-AQ data highlighted in this paper, i.e., less than 2 km altitude over the SMA (36.9–37.73 N, 126.65–127.83 E), this smoothing process contributed to 8% of the CO and CH_4 observations (consistent with the frequent calibration of the instrument every 5 min), 2.6% of the water vapor observations, and less than 2% of the O_3 and NO observations. This enabled just over 77,000 unique calculations accounting for 80% of the DC-8 flight time over the SMA.

This median smoothing process was also applied to the following non-critical constraints: CH_2O, PAN and methanol. These are species that can be calculated by the model if not available to constrain the calculations. Smoothed data contributed to roughly 4% of CH_2O, 9% of PAN, and less than 2% of methanol data used in the calculations enabling constraint of these species for all but a handful of model runs. In the case of H_2O_2 and HNO_3, the smoothing process was not effective in adding much additional information, but observations were still available to constrain over 80% of the model runs. Fortunately, constraining these species had a negligible effect on calculations for the conditions encountered over the SMA during the study period (see discussion in Section 4).

A final step in preparing the model inputs required special consideration for non-methane hydrocarbons. Fortunately a subset of important hydrocarbons were measured at 1 Hz: C_2H_6 by CAMS and aromatics and isoprene by PTR-TOF-MS (see **Table 1** for complete list). The large number of other hydrocarbon compounds were derived from whole air samples collected at discrete time intervals (see **Table 1** for details). For these species, "pseudo" 1 Hz interpolated values were derived using 1 Hz measurements of C_2H_6. Taking the ratio of each WAS measurement of C_2H_6 to the average of 1 Hz measurements during the WAS integration time resulted in a small correction factor for each sample. Taking these correction factors, the full timeline of 1 Hz C_2H_6, including time gaps between WAS samples, was normalized by applying the average ratio between consecutive samples from the middle of one sample integration period to the next. This "adjusted 1 Hz ethane" was then used to derive 1 Hz inputs for other WAS species having anthropogenic sources. For example, a "pseudo" 1 Hz propane input was derived by taking the propane-to-ethane ratio for each WAS measurement. These ratios were then applied to the "adjusted 1 Hz ethane" again using the average ratio between consecutive WAS samples from the middle of one sample integration period to the next. This scheme was applied to derive 1 Hz inputs for lumped C_{4+} alkanes, ethene, lumped C_{3+} alkenes, ethyne, and benzene. Similar to the correction of 1 Hz C_2H_6, isoprene measurements from WAS canisters and 1 Hz PTR-TOF-MS data were used to derive an "adjusted 1 Hz isoprene" input. PTR-TOF-MS measurements of toluene and C_8 aromatics were found to be in very good agreement with WAS measurements, so 1 Hz measurements of these species were used as-is for model inputs. Remaining VOC inputs, such as methanol and acetone, were only measured by PTR-TOF-MS and therefore used as-is for model inputs.

Model calculations of the free radical species that mediate ozone production allowed for the determination of instantaneous rates of net ozone production, $P(O_3)$, with individual terms given in the equation below.

$$P(O_3) = k[HO_2][NO] + \sum k_i[RO_2]_i[NO] - k[O^1D][H_2O] - k[O_3][OH] - k[O_3][HO_2] - k[OH][NO_2] - \sum k_i[O_3][NMHC]$$

The first two terms represent ozone formation from the conversion of NO to NO_2 by hydroperoxy (HO_2) radicals and the numerous organoperoxy (RO_2) radicals resulting from hydrocarbon oxidation. Loss terms include the reaction of O^1D from ozone photolysis with water, direct reaction of ozone with OH and HO_2, reaction of NO_2 with OH to form nitric acid (an indirect ozone loss via odd oxygen, $O_x \equiv O_3 + NO_2$), and ozonolysis reactions with hydrocarbon species.

As noted above, a minor adjustment to the model mechanism was made in response to the dominance of C_{7+} aromatic compounds in the SMA. In previously modeled environments, including airborne field campaigns

over remote areas and polluted cities in the USA, aromatic species had never played a dominant role. For example, the mean mixing ratio of C_{7+} aromatics below 1 km over Seoul during KORUS-AQ was a factor of five higher than observed below 1 km over Houston during the DISCOVER-AQ airborne campaign (Summer 2013). This led to scrutiny of the OH reaction rate constant for the lumped C_{7+} aromatic compounds (AROM) when initial model calculations produced unrealistic results for peroxyacetylnitrate (PAN) and CH_2O, indicating that the modeled radical environment (and modeled rate of $P(O_3)$) was also unrealistic. Specifically, using the original OH rate constant for C_{7+} aromatics led to model over-prediction of PAN in Seoul by a factor of 10–15 and CH_2O by a factor of 2–3. The rate constant, one of only a few still based on the Lurmann et al. (1986) lumped hydrocarbon mechanism, was found to significantly overpredict the rate of aromatic oxidation by OH when considering current literature for toluene and higher aromatic reaction rates. To best represent aromatic oxidation, the rate constant for AROM + OH was updated to take the following form:

$$k_{AROM+OH} = A * \left(1.8 \times 10^{-12}\right) * e^{(340/T)}$$

This equation combines the rate constant for toluene with a simple scaling factor, A, accounting for the ratio of C_8 aromatics to toluene for a given model run. The calculation of A took the following form:

$$A = \left(\left[C_8 \text{ aromatics}\right] * 2.43 + \left[\text{Toluene}\right]\right) / \left[\text{lumped } C_{7+} \text{ aromatics}\right]$$

The scaling factor of 2.43 was derived by assessing the relative OH reactivity of toluene versus C_8 aromatics ($k_{C8\ aromatics\ +\ OH}/k_{Toluene\ +\ OH}$) for the mean mixing ratios of aromatics measured in the whole air samples. For a scaling factor of A =1.4 (median value for calculated over Seoul) and a temperature of 298 K, the revised rate constant is about 50% lower than the original rate constant. In addition, the stoichiometric yields of glyoxal and methyl gloxal from C_{7+} oxidation under high-NO_x conditions have been adjusted from 0.18 and 0.72 to 0.27 and 0.3 to better-reflect results from chamber experiments (Tuazon et al., 1984; Smith et al., 1998) and to better agree with lumped chemical mechanisms used in 3D models, such as CAM-Chem (Louisa Emmons, private communication, 2018). These changes combined to lower the calculated $P(O_3)$ below 2 km over the SMA by an average of 20%, but at low altitudes over Seoul, where observations of C_{7+} aromatics were highest, these changes resulted in up to a 65% decrease in calculated $P(O_3)$. Outputs from all box model simulations are available on the KORUS-AQ archive: https://www-air.larc.nasa.gov/cgi-bin/ArcView/korusaq?MODEL=1.

4. Evaluation of model performance

To provide confidence in model-calculated rates of $P(O_3)$, which cannot be directly observed, an objective assessment of model performance is enabled by observed species that can either be used to constrain the model as an input or be calculated to be in photochemical steady state. Comparison of calculated and observed values for these test species can provide important insights on the aspects of the photochemistry that are being well represented and the sensitivity of the model to aspects that are not well represented. Limitations of the model are exacerbated for species with longer lifetimes, which are less likely to in photochemical steady state, and conditions under which physical processes such as transport, deposition, or wet removal are dominating over photochemistry. It is also useful to have a large number of observations over which to test model performance as there are many conditions that can perturb local steady state for individual runs but not induce a bias in the overall statistics. For instance, measurements in a partially cloudy field can have large fluctuations in measured photolysis frequencies. Radical species can rapidly respond to such fluctuations, but longer-lived species will not be in photochemical equilibrium, and will deviate from model predictions both positively and negatively. Because the destruction of some secondary species (such as CH_2O, PAN, H_2O_2, and HNO_3) provides chemical feedback into the modeled radical pool, over-prediction of these species by box models can have cascading effects on modeled rates of O_3 formation. The broad suite of measurements and the diverse set of chemical and meteorological conditions sampled during KORUS-AQ provide a unique platform to evaluate model performance and evaluate the importance of observing these species to constrain O_3 production estimates in a complex, heterogeneous megacity such as Seoul.

As noted in Section 3.2, model calculations were constrained by as many species as possible, including CH_2O, PAN, H_2O_2, and HNO_3 when measurements were available to allow for the most accurate representation of the feedback that these species provide. Although this set of highly-constrained calculations is expected to yield the most realistic estimates of radical abundances and rates of O_3 production, much can be learned about model sensitivity and local chemistry by comparing results of highly-constrained model runs to those using fewer constraints. For this comparison, four additional set of model calculations were performed. All inputs were identical to those in the highly-constrained set of runs, except each set left one of the secondary species unconstrained: CH_2O, PAN, H_2O_2, and HNO_3. The following discussion examines the comparison between model calculations for each of these species with their observed values, the reasons for differences, and the significance of these differences to model estimates of net O_3 production.

Figures 3, 4 and **5** examine observed versus calculated vertical profiles of H_2O_2, PAN, and CH_2O for the descents of the DC-8 over Seoul. Each figure is separated into morning, midday, and afternoon, showing how observed and modeled vertical profiles evolve throughout the day. The top row of each figure shows the statistics of observed vertical profiles, the middle row shows the ratio of modeled/measured mixing ratios from "unconstrained" calculations, and the bottom row shows the calculated lifetimes of the given test species. The diurnal evolution of ambient H_2O_2 in the top panels of **Figure 3**

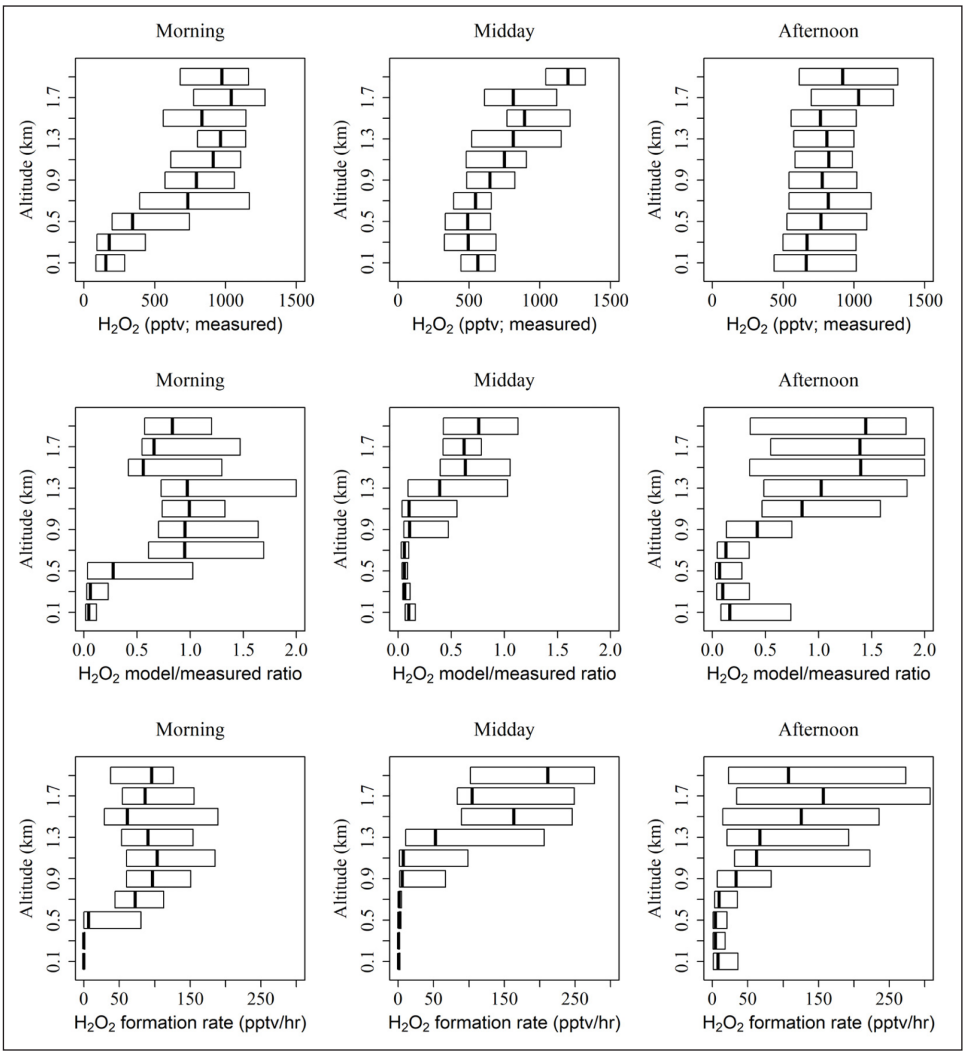

Figure 3: Vertical profiles of measured mixing ratios of H_2O_2 (top), the ratio of modeled/measured H_2O_2 from the "H_2O_2–unconstrained" set of simulations (middle), and the formation rate for H_2O_2 (bottom). All data and calculations are from DC-8 profile descents over Seoul, and are broken up to show diurnal trends across morning (left), midday (middle), and afternoon (right). All data were divided into 0.2 km bins, and the box and whisker plots represent the median value and interquartile range for each bin. DOI: https://doi.org/10.1525/elementa.400.f3

exhibits the combined influences of chemistry, deposition, and vertical mixing. In the morning, H_2O_2 was present in low amounts in the shallow boundary layer (median values below 200 pptv), while a reservoir of relatively high H_2O_2 (median values greater than 700 pptv) was present above 1 km. Here, we refer to the boundary layer as the lowermost region of the atmosphere that is directly impacted by surface emissions, which is typically very shallow (a few hundred meters) in the morning, and extends up to 1–2 km by the afternoon. The low mixing ratios of H_2O_2 in the morning boundary layer result from inhibited photochemical production of H_2O_2 as well as deposition throughout the night. Due to an overabundance of NO_x, photochemistry in Seoul was radical-limited during KORUS-AQ (described in greater detail in Section 5), which limits chemical formation of H_2O_2 since reaction of HO_2 with NO dominates over the HO_2 self-reaction. This is exacerbated in the morning, when low photolysis, low vertical mixing, and strong NO_x emissions would act to strengthen the radical-limited conditions. As the day progresses, mixing ratios of H_2O_2 at low altitudes increase, while mixing ratios aloft remain relatively constant. By the afternoon, there is little vertical gradient in H_2O_2; however, mixing ratios at lower altitudes never exceed those of the reservoir aloft. This behavior is consistent with H_2O_2 in the boundary layer over Seoul being largely driven by entrainment of air from the residual layer aloft. The vertical profiles of the ratio of modeled/measured H_2O_2 further support this hypothesis. Model/measured ratios of H_2O_2 at higher altitudes are closer to one than at low altitudes, indicating that the air in the residual layer is better described by the steady state assumption than air in the boundary layer. In the morning, for example, modeled/measured H_2O_2 ratios in the boundary layer were extremely low (below 0.1 at the lowest level), indicating model under-prediction of H_2O_2, while modeled/measured H_2O_2 ratios in the residual layer were typically between 0.5–1.5. The calculated lifetimes for H_2O_2 due to photochemical loss and deposition were on the order of 15–20 hrs and did not vary substantially with altitude. Comparatively, the H_2O_2 formation rates shown in **Figure 3** exhibited large gradients with altitude and was driven primarily by the abundance of NO. As the day progressed, this led to underpredictions

of H_2O_2 at higher altitudes as high NO values were mixed higher into the growing boundary layer. In effect, model calculations of H_2O_2 did not match measurements within the boundary layer because of the large variation in local formation rates versus the more dominant influence of vertical mixing (not accounted for in the model) delivering higher abundances of H_2O_2 produced aloft under conditions of much lower NO.

PAN, presented in **Figure 4**, exhibited small vertical gradients with higher mixing ratios tending toward lower altitudes. Values also increased throughout the day at all altitudes with afternoon values roughly double those observed in the morning. This behavior suggests that photochemical production from surface emissions drove the diurnal evolution of PAN observations. This is also consistent with the vertical gradient observed at midday when the boundary layer is still growing and the effect of surface emissions has yet to reach the top of the measured profile. Looking at modeled/measured mixing ratios, PAN was generally overestimated by the model, but the modest overestimates in the morning can be sharply contrasted with the large overestimates aloft later in the day. This model behavior can be best understood in the context of the PAN lifetime shown at the bottom of **Figure 4**. Model performance was best at the lowest altitudes where PAN lifetime was shortest and the expectation of steady-state the best. Nevertheless, the slight tendency to overestimate at these altitudes likely resulted from mixing of PAN from above where NO_x was less abundant, but the lifetime of PAN was longer. The highest modeled/measured ratios occurred between 400–800 m in the morning, between 900–1,400 m at midday, and between 1,200–2,000 m in the afternoon. These altitudes roughly correspond to the range of boundary layer heights for those times of day. Those altitudes correspond to the longest PAN lifetimes in the profile that also have enough NO_x to sustain a large PAN production rate. Also note that the largest discrepancies occur at the highest (coldest) altitudes only when sufficient NO_x has mixed to those altitudes. As was the case for H_2O_2, these model discrepancies are ultimately caused by the vertical mixing that is not represented in the model. For PAN, it is the mixing from below that prevents the build-up of PAN to steady-state values at higher altitudes where PAN lifetimes are longer than the timescale for mixing. The widening of the range of modeled/measured PAN ratios at higher altitudes also reflects daily variability in the boundary layer height. For example, during Research Flight 7, the top of the boundary layer at midday was 1.5 km (as indicated by

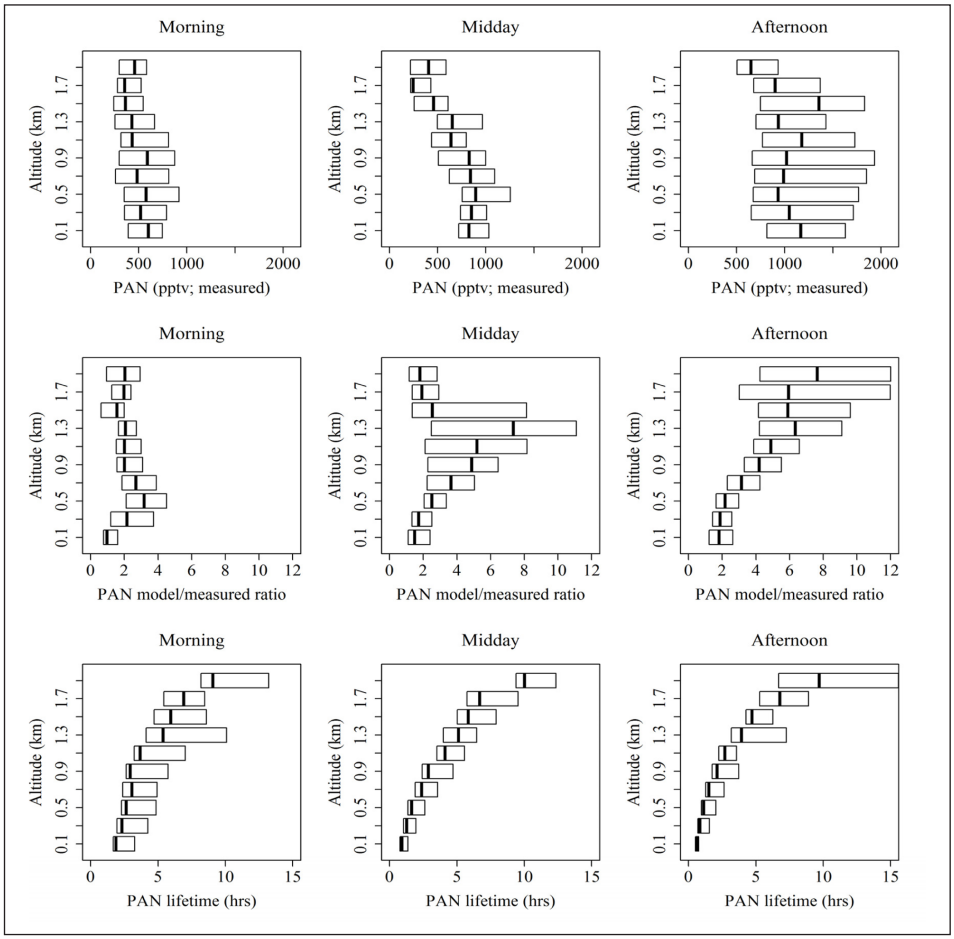

Figure 4: Vertical profiles of measured mixing ratios of PAN (top), the ratio of modeled/measured PAN from the "PAN_unconstrained" set of simulations, and the calculated lifetime of PAN. All data and calculations are from DC-8 profile descents over Seoul, and are broken up to show diurnal trends across morning (left), midday (middle), and afternoon (right). All data were divided into 0.2 km bins, and the box and whisker plots represent the median value and interquartile range for each bin. DOI: https://doi.org/10.1525/elementa.400.f4

gradients in the test species and other short-lived species, such as NO_x). During this time, the model/measured ratio increased with altitude before reaching a maximum value at 1.5 km, coincident with the top of the boundary layer. During Research Flight 10, on the other hand, the top of the boundary layer at midday was 1.3 km, and the maximum PAN modeled/measured ratio occurred at this height as well.

The vertical profiles of CH_2O presented in **Figure 5** also indicate photochemical production within the mixed layer. However, in contrast to PAN, model calculations of CH_2O reasonably match observations at all altitudes and all times of day. One reason for this can be attributed to the much shorter calculated lifetimes for CH_2O over Seoul which also had much less vertical variability than calculated PAN lifetimes; thus, the expectation for CH2O to approach steady-state is much greater for CH_2O than either H_2O_2 or PAN. Because CH_2O is closely related to the rate of VOC oxidation and the abundance of radical species (Wert, 2003; Parrish et al., 2012; Valin et al., 2015; Schroeder et al., 2016; Wolfe et al., 2016), model-measurement agreement indicates that the VOC mixture used to constrain the model and the underlying chemical mechanism are adequate to represent of ambient conditions for CH_2O.

HNO_3 (not shown) is another secondary species that was calculated in an unconstrained simulation. Modeled HNO_3 consistently exceeded observations by greater than a factor of 10 within the boundary layer. This can be attributed in part to the lack of adequate sinks in the model, which did not account for uptake of HNO_3 to form particulate nitrate.

Having shown that the steady-state assumption is inadequate for describing some species in Seoul, it is important to assess the associated feedbacks that these species have on modeled rates of net O_3 production, $P(O_3)$, in Seoul. In addition to the previously-described sets of model calculations, an additional set simulations were run whereby all four test species were unconstrained. Comparison of these six sets of simulations (constrained,

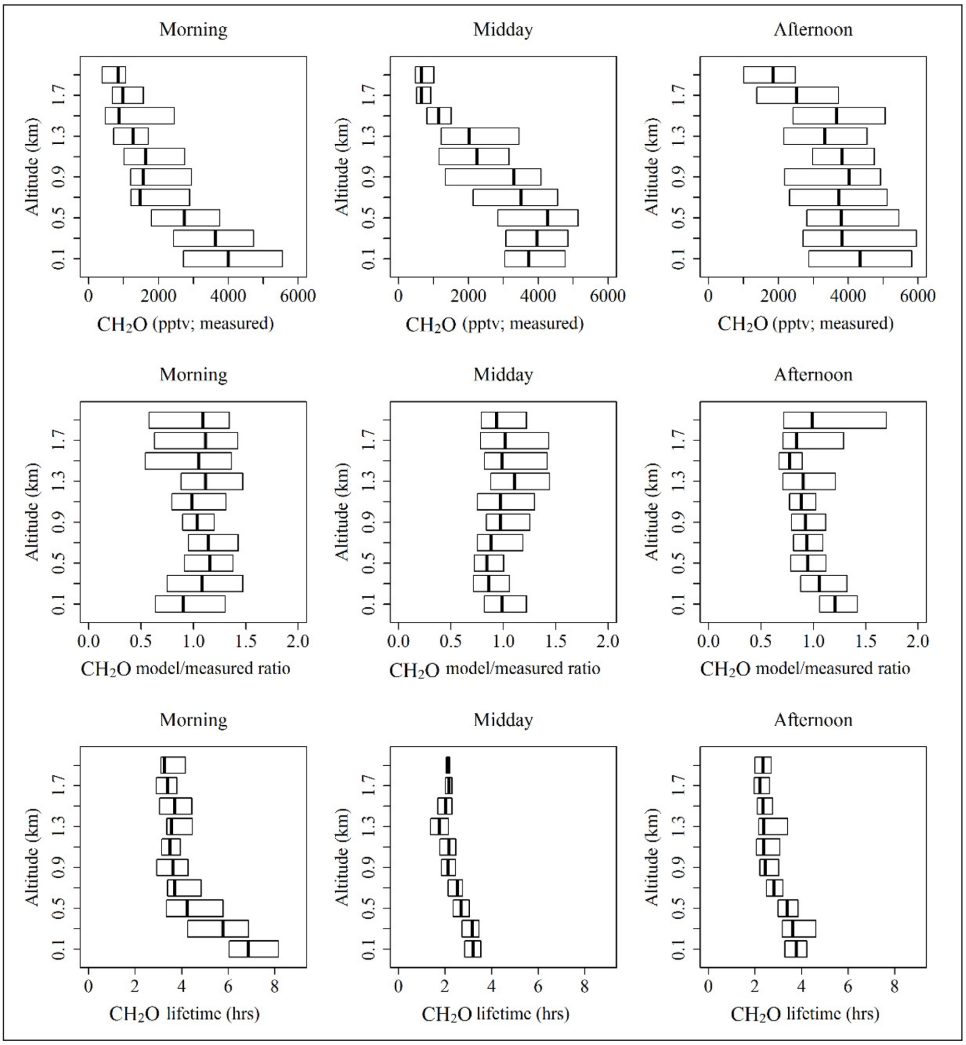

Figure 5: Vertical profiles of measured mixing ratios of CH_2O (top), the ratio of modeled/measured CH_2O from the "CH_2O_unconstrained" set of simulations, and the calculated lifetime of CH_2O. All data and calculations are from DC-8 profile descents over Seoul, and are broken up to show diurnal trends across morning (left), midday (middle), and afternoon (right). All data were divided into 0.2 km bins, and the box and whisker plots represent the median value and interquartile range for each bin. DOI: https://doi.org/10.1525/elementa.400.f5

unconstrained, and the four simulations with each species unconstrained individually) allows for such an evaluation. **Figure 6** shows cumulative distributions of calculated $P(O_3)$ from each of these model simulations. Between the constrained (black line) and unconstrained (gray line), there is a shift towards higher rates of $P(O_3)$ in the unconstrained runs. To understand this difference, these two sets of model runs are compared with those for each of the individually unconstrained species runs. A quick examination shows that the difference is entirely due to the constraint of PAN. This is due to the additional production of organic peroxy radicals resulting from the overpredicted PAN abundances in the unconstrained runs. The lack of model sensitivity to H_2O_2 and HNO_3 is due to their weak roles as radical reservoirs in the polluted Seoul environment such that radical abundances and resulting rates of O_3 production do not rely on their being well-represented in the model. Conversely, CH_2O is a strong peroxy radical source, but it is generally well predicted by the model with model/measurement discrepancies that are evenly distributed around the observed values. Thus, differences in individual model runs between constrained and unconstrained calculations do not affect the overall distribution of $P(O_3)$. While it is difficult to quantify specifically, it is expected that the interpolation of hydrocarbon observations makes a large contribution to the discrepancies for individual model calculations while having no detectable impact on the aggregated statistics.

The exercises described above serve to highlight the importance of having a wide suite of measurements to constrain a box model in heavily polluted environments. In complex environments such as Seoul, where a confluence of strong time-varying local emissions, local meteorology, and background or residual pollution act to reduce the applicability of the steady-state assumption, the importance of model constraints is very high. In this case, without measurements of PAN to constrain the model, calculated rates of $P(O_3)$ in Seoul would be biased high by more than 40% when integrated over the distribution of calculated rates.

This bias related to overprediction of PAN is of particular concern given the intent to use the model to examine the sensitivity of $P(O_3)$ to changes in precursors. Such calculations must be conducted without constraining PAN

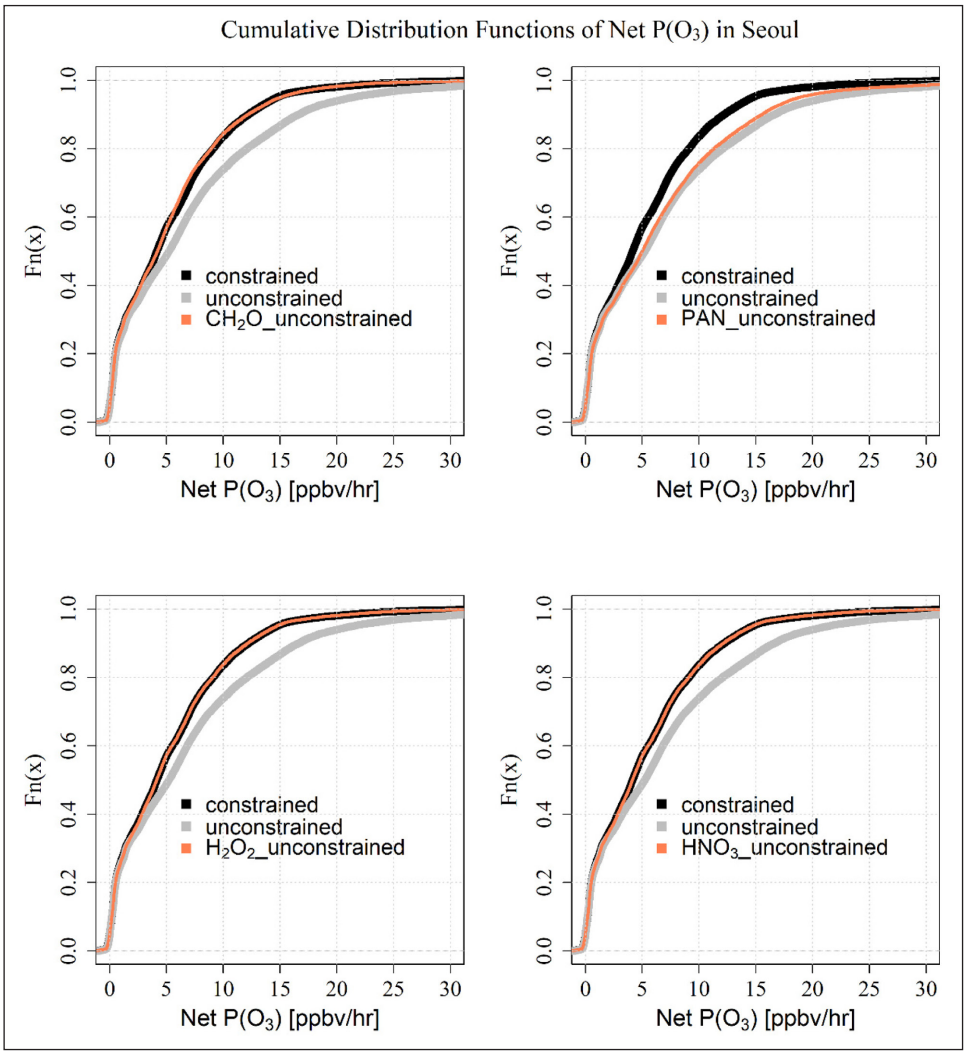

Figure 6: Cumulative distribution functions from different simulations using inputs derived from profile descents over Seoul. The same set of model inputs were used for each simulation, but the number of species used to constrain the model was varied between simulations, as indicated by the legend. DOI: https://doi.org/10.1525/elementa.400.f6

as its abundance must be allowed to change along with precursors. While the reason for the PAN discrepancy is tied to the physical process of boundary layer mixing, it is necessary to represent this impact in the box model with a chemical analog. As noted earlier, the strong temperature dependence of PAN thermal decomposition leads to a large range of lifetimes for PAN (e.g., up to 10–15 hours near 2 km as shown in **Figure 4**). Such lifetimes are unrealistic, given the expectation of a much shorter time for vertical mixing in the boundary layer; thus, a first-order loss of PAN was introduced into the model that was based on thermal decomposition at the average temperature in the lowest 2 km during daily descents over Seoul. Given both daily and diurnal temperature changes, the average temperature was determined for each individual descent over Seoul to determine the first order loss rate to apply to each data point. This loss was calculated to be half the rate of thermal decomposition at the average temperature for the profile below 2 km. This first-order loss is artificial in that it represents nonlocal decomposition as air is vertically exchanged, acting to limit the buildup of PAN at higher altitudes where lifetimes were too long and also effecting minor reductions of PAN at lower altitudes where precursor abundances were much higher than other altitudes in the boundary layer profile. This procedure was applied not only to PAN, but also to other peroxyacyl nitrates in the model (e.g., PPN derived from alkanes, TPAN derived from aromatics, and MPAN derived from isoprene).

Conducting unconstrained model calculations with this additional loss term for peroxyacyl nitrates had a dramatic impact on model performance. The regression of model-calculated PAN against observations improved substantially, showing both a reduction in the bias and an improvement in the correlation between calculated and observed PAN. The PAN regression slope for Seoul decreased from 4.8 to 0.92, the intercept changed from –50 to –25, and the R^2 increased from 0.33 to 0.49. The constrained calculations were also adjusted to include the new treatment of other peroxyacyl nitrates (PPN, TPAN, and MPAN), resulting in an 11% reduction in the integrated ozone production shown in **Figure 6**. Most importantly, the bias in ozone production between constrained and unconstrained calculations was dramatically reduced with integrated ozone production for the unconstrained calculations being only 8% lower than the constrained calculations. This modification to the model as applied to KORUS-AQ conditions allows for a more confident analysis of ozone production sensitivity to precursors, which is pursued in subsequent sections.

A final point of comparison is obtained by comparing calculated rates of net O_3 production to observed changes in O_3. For this comparison, results from the constrained set of model runs (with updated treatment of peroxyacyl nitrates) are examined for the repeated profiling by the DC-8 over Seoul during the descents over Olympic Park which consistently sampled the same ground track from an altitude of 1 km down to a few tens of meters above the surface.

Table 3 shows statistics for average O_x, O_3, and model-calculated $P(O_3)$ from the morning, midday, and afternoon descents over Seoul. From the morning to midday, an average change of 17 ppbv of O_x (16 ppbv of O_3) over a period of 3.5 hours yields an observed rate of change of O_x (and O_3) of ~4.8 ppbv/hr, compared to the average calculated $P(O_3)$ between morning and midday of 5.6 ppbv/hr. Likewise, from midday to afternoon, the observed change of 16 ppbv of O_x (20 ppbv of O_3) over a period of ~3.5 hours yields an observed rate of change of O_x of ~4.6 ppbv/hr (and ~5.7 ppbv/hr for O_3) compared to the average calculated $P(O_3)$ between midday and afternoon of 7.8 ppbv/hr.

Table 3: Column averaged values of observed O_x (O_3 in parentheses) and modeled $P(O_3)$ below 1 km during Seoul missed approach profiles. DOI: https://doi.org/10.1525/elementa.400.t3

Profile Time	Average O_x (O_3) [ppbv]	Average $P(O_3)$ [ppbv/hr]	Average local time
Morning	71 (59)	3.2	08:25
Midday	88 (75)	8.1	12:06
Afternoon	104 (95)	7.5	15:29

These aggregate statistics demonstrate the strong role of photochemistry in the O_3 changes observed over Seoul. It is also important, however, to recognize that other influences on O_3 such as advection, entrainment from above, and surface deposition are not represented in the box model. Each of these factors should reduce O_3 on average since Seoul is a strong source region and may explain the higher calculated rates of production as compared to observed changes.

5. O_3 Sensitivity in the SMA

Understanding O_3 sensitivity, that is, whether local O_3 production is NO_x-limited or radical-limited (VOC-limited), is a critical step towards drafting effective mitigation policies. During KORUS-AQ, DC-8 flights took advantage of natural gradients in O_3 and its precursors by repeatedly overflying Seoul and Taehwa forest, located ~30 km to the southeast, on many different days and under different conditions. A summary of these DC-8 observations for altitudes below 1 km is shown in **Figure 7**, contrasting data from the overflight of the two sites in the morning, midday, and afternoon. The most noticeable difference is that NO_x mixing ratios were always lower over Taehwa than over Seoul at all times of day with median values that were 2-6 times lower over Taehwa, Seoul also exhibited a much wider range of extreme values, especially in the morning when emissions were concentrated near the surface before substantial boundary layer growth had occurred. NO_x levels were lower outside the city due to dilution of the primary emissions as they moved downwind, as well as chemical processing. By contrast, CH_2O, an excellent proxy for VOC chemistry, was very similar between the two sites (with the exception of Taehwa in the morning), and roughly constant throughout the day. This is consistent with the continuous oxidation of VOCs and the short lifetime of CH_2O. The lower morning CH_2O at Taehwa also suggest a role for biogenic VOC emissions which increase throughout the day with temperature. O_3 and O_x increased stead-

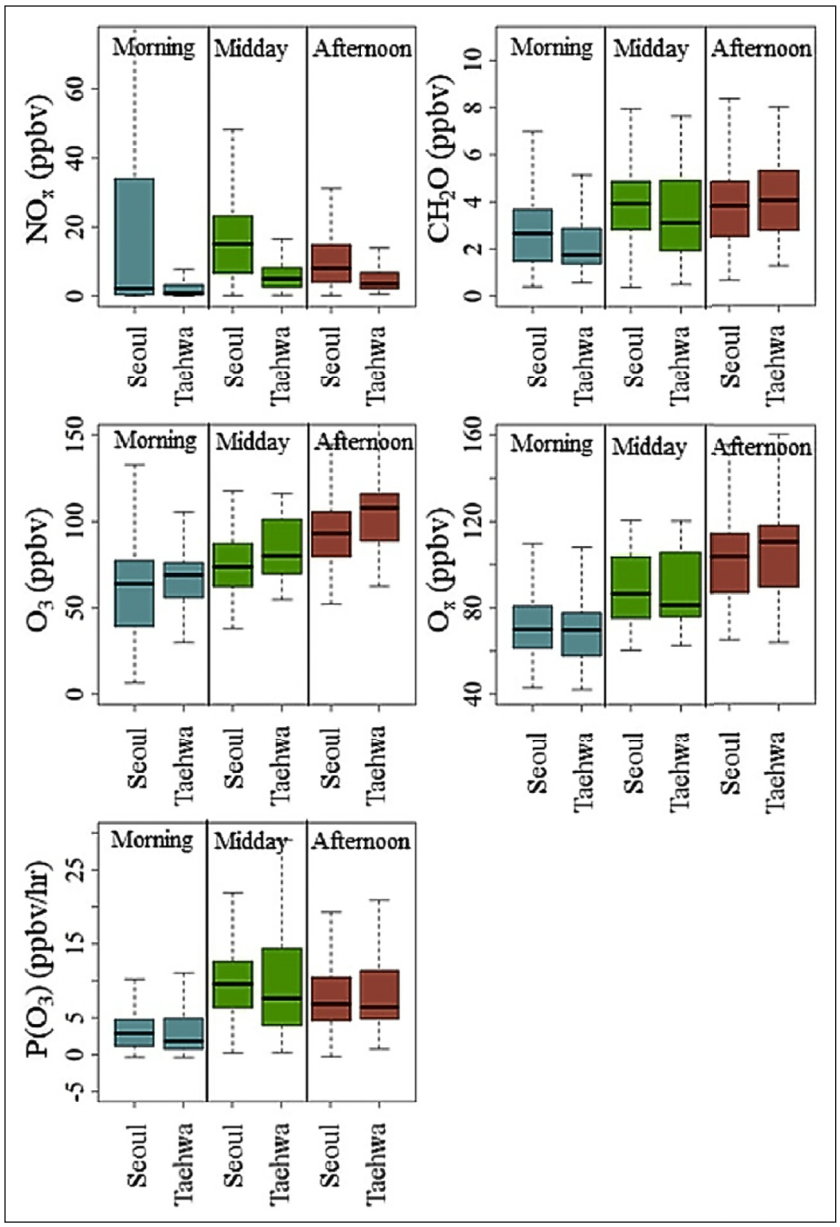

Figure 7: Diurnal distributions of observed NO_x, CH_2O, O_3, O_x and modeled $P(O_3)$ over Seoul and Taehwa. Distributions are represented as box-whisker plots, where the thick black line represents the median value, the bounds of the box represent the interquartile range, and the whiskers represent the 5th and 95th percentiles. DOI: https://doi.org/10.1525/elementa.400.f7

ily from morning to afternoon at both sites, consistent with a photochemical source. While O_x distributions were similar, O_3 tended to be higher over Taehwa in relation to Seoul due to the partitioning between O_3 and NO_2 under the high NO_x conditions in Seoul. The bottom left panel in **Figure 7** shows net O_3 production rates calculated from the constrained set of model runs. Compared to the observed quantities, $P(O_3)$ behaves most like CH_2O, as both map closely to photochemistry with lower morning values versus midday and afternoon. The lack of change in $P(O_3)$ across the large NO_x gradient demonstrates the NO_x-saturated behavior in the model calculations. This allows sustained ozone production to increase both O_3 and O_x across the region throughout the day. Thus, these observations provide a natural experiment whereby O_3 production is sustained over a large NO_x gradient, without an associated gradient in VOCs (based on the CH_2O proxy), demonstrating that O_3 production across the SMA was radical-limited (i.e. VOC-limited or NO_x-saturated). This builds upon recent work by Kim et al., (2018), who used measurements from an instrumented ground site in Seoul to identify conditions as radical-limited, by using airborne measurements throughout the boundary layer over a large area to understand O_3 sensitivity over the broader SMA.

5.1. Model sensitivity to VOC classes

The findings highlighted in the previous section indicate that effective O_3 mitigation strategies in the SMA must include reductions in VOC emissions. However, because VOCs as a class contain a broad spectrum of different species with a wide range of reactivities and radical yields, exploring the contributions of individual VOCs or classes of VOCs to the overall rate of O_3 production is a crucial next step towards identifying emissions sectors that contribute

disproportionately to O_3 production. To better understand the sensitivity of O_3 to specific VOC classes, additional box model simulations were conducted whereby select VOC constraints were set to zero in the model. For these simulations, the model was not constrained by observations of CH_2O, PAN, HNO_3, and H_2O_2 because of the associated feedback that removal of VOCs would have on these species. **Figure 8** shows the distribution of calculated O_3 production rates over Seoul using a complete suite of DC-8 observations (black dashed line) compared to simulations where a single hydrocarbon or group of hydrocarbons were removed from the model (orange line in each panel). Note that because of the complex feedback that VOCs have on radical abundances and HO_x/NO_x partitioning, the percent reductions shown in **Figure 8** do not add up to 100%. The general shape of the $P(O_3)$ distribution in the black dashed line (i.e. base-case) shows two distinct modes: one centered around 0–1 ppbv/hr and one centered around 4–5 ppbv/hr. In general, the lower mode contains data collected in the morning, at higher altitudes (1–2 km), and features low concentrations of NO_x (mean 0.3 ppbv) and low concentrations of short-lived hydrocarbons (for example, a median isoprene concentration of 0). The data that make up this mode are characterized as clean or aged airmasses above the boundary layer that were not recently impacted by surface emissions. The second mode, centered around 4–5 ppbv/hr, features data that contain characteristics of urban pollution, with relatively high NO_x (mean 11 ppbv) and VOCs.

C_{7+} Aromatic compounds (which include toluene, ethylbenzenes, and xylenes) are shown to have the greatest impact on modeled O_3 production, with a 32% reduction in mean $P(O_3)$ and a sharp change in the distribution, with a large reduction in the amount of data falling above 5 ppbv/hr. Modeled O_3 production was also fairly sensitive to isoprene, with removal of isoprene yielding a 15% reduction in mean $P(O_3)$ over Seoul. Alkenes (which include ethene, propene, C_4 alkenes, and C_5 alkenes) also were found to contribute an important amount to O_3 production in Seoul, with removal of alkenes resulting in a 14% reduction in mean $P(O_3)$. In contrast to C_{7+} Aromatics, removal of either isoprene or alkenes from the model resulted in little change in the modeled distribution of $P(O_3)$ above 5 ppbv/hr. In effect, removing C_{7+} Aromatics from the model had a large effect on points with very high values of $P(O_3)$, while removing isoprene or alkenes tended to mostly impact points that were producing below 5 ppbv/hr in the base-case simulation. Other VOCs, including light alkanes, heavy alkanes, methanol, and CO (not shown) had negligible effect on modeled $P(O_3)$. **Figure 8** shows results of sensitivity simulations over Seoul, but similar results were noted when the study area was expanded to the entire SMA: Removal of C_{7+} Aromatics yielded a 36% reduction in mean $P(O_3)$, isoprene a 13% reduction, alkenes a 13% reduction, and all other species yielded 7% or less. Additionally, the results shown in **Figure 8** include all data collected below 2 km, which may mask the contribution of very short-lived VOCs, like isoprene, which have vertical profiles that are weighted towards the surface. When data are filtered to only include data collected below 1 km over Seoul, the percent reductions in mean $P(O_3)$ become 34% (C_{7+} Aromatics), 16% (isoprene), 13% (alkenes), 3% (C_{4+} alkanes), 1% (light alkanes), and 6% (methanol). Thus, no matter how the data are filtered (Seoul only, whole SMA, low altitudes only, etc.), the results suggest that reductions in anthropogenic emissions, particularly C_{7+} Aromatics (and alkenes, to a lesser extent), could provide an attractive target for reductions in local O_3 production. This finding will benefit from source apportionment work being conducted by other KORUS-AQ investigators to characterize sources and quantify emissions of these species in the SMA. By contrast, the natural source of isoprene from vegetation does not offer an effective target for emissions reduction but must be considered to understand the response of O_3 chemistry to emissions reductions for anthropogenic VOCs.

5.2. Model sensitivity to NO_x reductions

While reductions in C_{7+} aromatics would benefit local O_3 production in Seoul, the regional extent of downwind production must also be considered. The higher levels of O_3 and $P(O_3)$ at Taehwa (see **Figure 7**), despite the lower concentrations of NO_x, highlights the regional impact that the very high NO_x in Seoul has on sustaining O_3 production downwind and across the surrounding region. Thus, despite the large gradient in NO_x from inside Seoul and into the surrounding region shown in **Figure 7**, conditions remain conducive to high rates of O_3 production over a very large area and the only way to limit the regional extent of ozone production is to also target NO_x emissions for reduction.

In a strongly radical-limited environment, initial reductions in NO_x for a given VOC abundance will result in an increase in $P(O_3)$. After a sufficient amount of NO_x is removed, modeled $P(O_3)$ will reach a maximum at the point where O_3 sensitivity transitions to a NO_x-limited environment. Further reductions in NO_x beyond this point result in decreases in $P(O_3)$ relative to the maximum, though $P(O_3)$ may still be higher than at the starting point. To assess the impact of NO_x reductions, model sensitivity to NO_x was evaluated using three additional simulations whereby model input values for NO were reduced by 25%, 50%, and 75% while all other inputs were kept the same. Two additional simulations were performed where NO_x and all relatively-short-lived anthropogenic VOCs (i.e. all VOCs except methane, CO, and isoprene) were reduced by 10% and 25%. **Table 4** shows the mean relative increase in modeled $P(O_3)$ from these experiments, filtered to show data from the entire SMA, Seoul, and non-Seoul SMA below 2 km. Over the entire SMA, reducing model input NO by 25% yielded a mean relative increase in modeled $P(O_3)$ by 5%, becoming 11% when NO was reduced by 50%. Upon reducing input NO by 75%, $P(O_3)$ was still higher than the base simulation by 10% on average, but was slightly lower than the simulations where NO was reduced by 50%. This indicates that, aggregated over the entire SMA, O_3 sensitivity changed from radical-limited to NO_x-limited over this experimental range of NO reductions. In simulations where both NO_x and VOCs were reduced, mean $P(O_3)$ decreased relative to the base simulation, demonstrating the value in concurrent reduction in emissions for both.

Table 4: Sensitivity of modeled $P(O_3)$ to reductions in input NO, shows as mean relative increases compared to base simulations (i.e. unchanged DC-8 observations). Data are filtered to compare sensitivity of $P(O_3)$ to NO_x over the entire SMA, Seoul, and non-Seoul SMA.

	Mean Relative Change in Modeled $P(O_3)$		
Model Simulation	**All SMA <2 km**	**Seoul <2 km**	**non-Seoul SMA <2 km**
NO −25%	+5%	+7%	+4%
NO −50%	+11%	+22%	+6%
NO −75%	+10%	+43%	−4%
NO + VOC −10%	−1%	−2%	−2%
NO + VOC −25%	−3%	−6%	−6%

When only data from urban Seoul are considered, reductions in NO always lead to an increase in $P(O_3)$, with the percent increase becoming higher with each subsequent NO reduction. This indicates that even with a 75% reduction in NO, the photochemical environment in urban Seoul is largely radical-limited. Interestingly, the changes in $P(O_3)$ from urban Seoul suggest that it is substantially more radical-limited than the SMA taken as a whole. Because of this, suppression of radicals (and $P(O_3)$) in urban Seoul leads to a lower base-case $P(O_3)$ compared to the entire SMA, and therefore a larger relative increase in $P(O_3)$ as the photochemical environment approaches the transition point where O_3 production is most efficient When only non-Seoul data were considered, the calculated mean relative increases in modeled $P(O_3)$ with NO reductions were lower than the other two datasets (i.e. all SMA and urban Seoul), and the mean relative change in $P(O_3)$ finally goes negative with the −75% simulation. As such, the "starting point" in the base-case simulation for non-Seoul was closer to the photochemical transition point than all SMA or urban Seoul.

These observations, combined with the results presented in Section 5.1, might suggest that reductions in VOC emissions should be a sole priority for reducing O_3 in the SMA, and that reductions in NO_x emissions would exacerbate the problem. While reducing NO_x in our simulations resulted in increases in modeled $P(O_3)$ in all but one case, it is also important to consider the associated feedbacks on key O_3 precursors, particularly NO_x itself. Because NO_x has a lifetime on the order of hours, ambient NO_x mixing ratios are the result of a balance between NO_x emissions and NO_x removal. While reductions in NO_x emissions would certainly lead to reductions in ambient NO_x mixing ratios, we must also consider how the lifetime of NO_x changes in response to associated changes in the photochemical environment. **Table 5** shows weighted averages of instantaneous NO_x lifetimes as calculated by our model, assuming that formation of HNO_3 is the only NO_x removal process. Reductions in constraining NO resulted in generally lower NO_x lifetimes compared to the base-case simulation, with the −75% simulation in urban Seoul yielding the largest reduction: a 66% decrease in the NO_x lifetime relative to the base-case simulation. This is important for two reasons: 1) Reduction in NO_x emissions will result in amplified reductions in ambient NO_x mixing ratios (for example, a 25% reduction in NO_x emissions should be expected to produce ambient NO_x reductions in excess of 25%, all else being equal, because of associated reduction in the NO_x lifetime), and 2) A shorter duration of O_3 production as airmasses move downwind from urban Seoul. While select VOCs, such as isoprene, are very short-lived, the majority of VOCs that were abundant in Seoul have lifetimes that are longer than NO_x, including aromatics (toluene, for example, has a lifetime of 1–2 days). In an environment such as the SMA, where VOCs are dominated by aromatics and emissions of biogenic VOCs persist throughout the region, the duration of O_3 production for a given polluted airmass as it moves downwind is essentially limited by the lifetime of NO_x in that airmass. Therefore, even though reductions in NO resulted in increased rates of O_3 production throughout the SMA in our simulations, the regional extent of O_3 production would be reduced. In **Figure 7**, we showed that a receptor site at Taehwa Forest consistently had lower NO_x mixing ratios than urban Seoul. If NO_x mixing ratios in urban Seoul were reduced by some amount, NO_x mixing ratios at receptor sites such as Taewha would be expected to be reduced by a larger amount, since a higher percent of NO_x would be chemically removed while in transit (owing to the shorter NO_x lifetime). In effect, while reductions in NO_x emissions could result in locally higher rates of O_3 production in urban Seoul, regions outside of urban Seoul should benefit if the associated NO_x reductions push them far enough into the NO_x-limited regime. Fully quantifying the effects of NO_x reductions on O_3 throughout the SMA requires the use of 3D models that can account for emissions, transport, and chemistry, and is beyond the scope of this work, but this question is being pursued by other KORUS-AQ investigators (Oak et al., 2019).

Table 5: Weighted average instantaneous NO_x lifetimes (hours), weighted by $F(O_0)$.

	weighted average of τ_{NOx} (hrs), weighted by $F(O_3)$		
Simulation	**All SMA <2 km**	**Seoul <2 km**	**non-Seoul SMA <2 km**
Base	7.7	11.6	6.1
−25%	6.0	8.2	5.0
−50%	4.7	5.7	4.2
−75%	4.0	4.1	4.0

6. Summary and Conclusions

As South Korea has experienced rapid industrial growth over the past few decades, exposure to unhealthy levels of O_3 has emerged as a public health concern, particularly in the SMA (population 25 million). Data collected by a network of ground stations in the SMA during KORUS-AQ indicated that O_3 exceed the Korean 8-hour AQS value on 39 days during the 41-day study period.

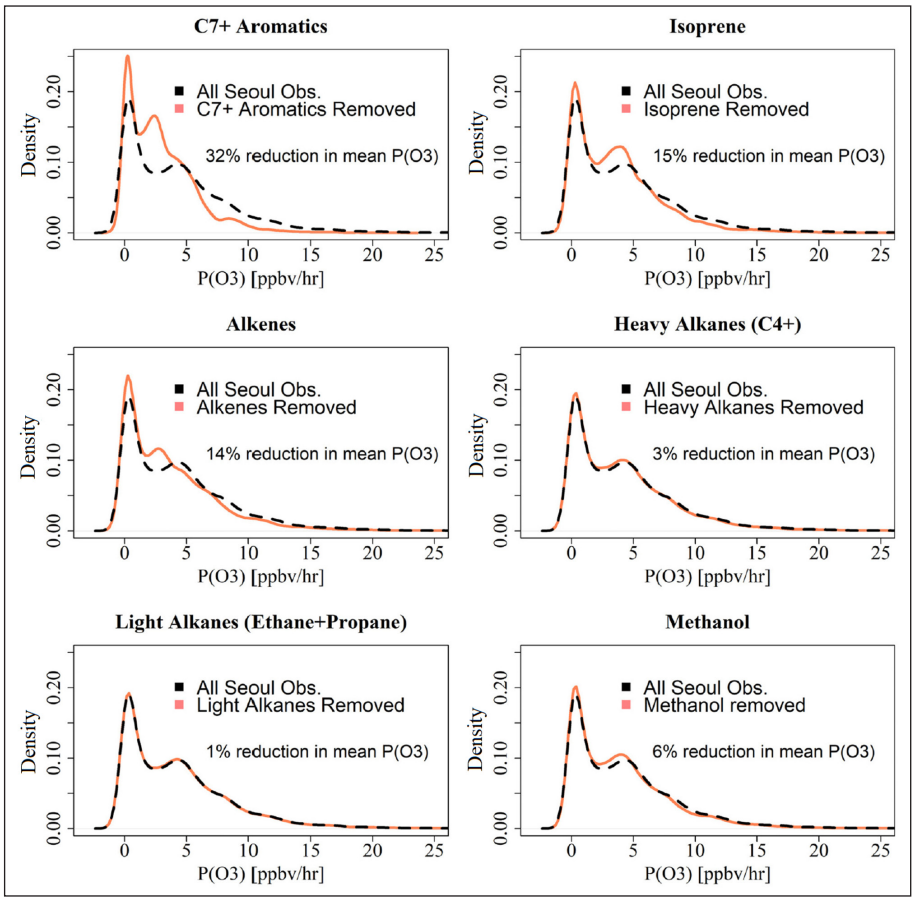

Figure 8: Modeled distributions of $P(O_3)$ over Seoul from the "base case" simulation (black dashed line in each panel), and from the zero-out simulation shown in each panel (orange line). DOI: https://doi.org/10.1525/elementa.400.f8

Furthermore, O_3 was observed to be highest in outlying suburban regions, particularly Gyeonggi province, rather than urban Seoul. In this work, airborne observations of O_3 and other trace gases were used alongside an observationally-constrained 0-D photochemical box model to explore the sensitivity of O_3 to changes in its precursors. The fidelity of these photochemical calculations was explored using a series of additional simulations, and it was found that the steady state assumption used in 0-D box models cannot describe select intermediate species, particularly PAN, H_2O_2, and HNO_3, while ambient CH_2O observations were well-represented by our model. Model shortcomings in the prediction of H_2O_2 and HNO_3 had no impact on model-calculated rates of O_3 production, while model results not constrained by PAN observations overpredicted average O_3 production in Seoul by more than 40%. This was mitigated by introducing a first order loss for PAN and other thermally labile peroxyacyl nitrates based on the average temperature in the boundary layer profiles of Seoul, providing much better agreement between constrained and unconstrained calculations of O_3 production. When fully constrained, aggregate statistics for model-predicted rates of O_3 production agreed well with average observed changes in ambient O_3.

Observed gradients in O_3 and its precursors between urban Seoul and a downwind receptor site (Taehwa Forest) indicated that O_3 production in the SMA was radical-limited (i.e. VOC-limited) over the study period. Additional zero-out simulations were performed whereby select VOCs were removed from the model, allowing for diagnosis of model sensitivity to individual VOCs. These simulations identified C_{7+} aromatics (i.e. toluene, xylenes, ethylbenzenes, etc.) as the dominant VOC contributor to O_3 production in the region, with a 32% reduction in mean O_3 production calculated when C_{7+} aromatics were removed from the model. Isoprene was found to be the second most important VOC with respect to contribution to O_3 production (15% reduction in mean O_3 production), and anthropogenic alkenes were the third most important (14% reduction in mean O_3 production).

Though the SMA was identified as radical-limited, analysis of model simulations in which NO_x was reduced provided insight on competing effects. When constraining NO was reduced by up to 75% in our model, O_3 production increased in Seoul but began to decrease for the surrounding area. Thus, areas outside of Seoul were found to transition from a radical-limited to a NO_x-limited environment within the range of NO_x reductions studied here, while urban Seoul remained radical-limited even at a 75% reduction in constraining NO. Furthermore, we found that in all regions of the SMA, reductions in constraining NO lead to decreases in the modeled NO_x lifetime. The results of a shortened NO_x lifetime could be two-fold: 1) as the plume from urban Seoul moves downwind towards receptor sites, the time-duration over which that plume is capable of producing high amounts of O_3 would be shortened, and 2) reductions in NO_x emissions should be accompanied by reductions in the NO_x lifetime, meaning

that for a given reduction in NO_x emissions, a larger decrease in ambient NO_x mixing ratios could be expected. These results indicate that, even though the SMA was identified as radical-limited, reductions in NO_x emissions would have complex effects on O_3 in the SMA, whereby O_3 in urban Seoul would likely increase as a result of reduced NO_x emissions, but regions outside of urban Seoul, particularly Gyeonggi province, could benefit. Additional benefits of NO_x reductions include reductions in ambient NO_2 (which is a criteria pollutant itself), and potential for reductions in fine particulate matter. However, analysis of these co-benefits is beyond the scope of this work.

The policy implications of this work are clear: reductions in VOCs, particularly C_{7+} aromatic compounds, provide an effective pathway for reducing O_3 production in the SMA. Anthropogenic alkenes, such as ethylene and propylene, also provide an attractive target for emissions reductions, but certainly should not be prioritized over C_{7+} aromatics. Isoprene, while an important contributor to O_3 production, does not represent a viable target for emissions reductions, owing to the biogenic nature of its source. The KORUS-AQ dataset can be utilized to classify and quantify sources of VOCs in the SMA, which may provide fruitful information for policymakers in drafting targeted mitigation strategies aimed at specific emissions sectors. Although O_3 production in the SMA is radical-limited, reductions in NO_x emissions should also be considered with the intent of reducing the regional extent of O_3 production. Broad-scale measurements of VOCs and NO_x in the SMA must be continued to understand changes in source contributions throughout the year, and to understand the effectiveness of any policies that are implemented. Long-term ground-based studies could provide continuous measurements at discrete locations, and follow-up airborne studies could be leveraged to explore emissions trends and gradients over larger spatial scales. While the O_3 sensitivity analysis provided in this work and other studies that analyze in-situ measurements from KORUS-AQ can point to specific emissions sources that would make for attractive targets for emissions reductions, fully understanding the effects of emissions reductions on future air quality requires the use of 3D models that implement emissions, transport, and chemistry. Because of this, it is imperative that the emissions parameterizations used in 3D models are realistic, and the measurements from KORUS-AQ can provide an attractive dataset to test and validate 3D models. Additional studies that compare the chemical mechanisms used in 3D models and other models (such as the LaRC box model used in this study) may also highlight potential strengths or shortcomings of the underlying chemical mechanisms used in 3D models. If veracity can be obtained for modeled emissions and chemistry, a larger degree of confidence in the outcomes of simulations with different emissions reductions scenarios can be gained.

Data Accessibility Statement

Outputs from all box model simulations used in this work are available on the KORUS-AQ archive: https://www-air.larc.nasa.gov/cgi-bin/ArcView/korusaq?MODEL=1.

Acknowledgements

The KORUS-AQ study was jointly funded by NASA and the Korean National Institute of Environmental Research (NIER). Special thanks goes to all who made the DC-8 flights over Seoul and in Korean airspace possible. This includes civil and military air traffic coordinators, DC-8 pilots and crew, and the scientists who negotiated the flight paths and permissions needed to collect these observations. The members of the PTR-MS instrument team (P. Eichler, L. Kaser, M. Müller) are acknowledged for their support with instrument preparation and field work.

Funding information

PTR-ToF-MS measurements aboard the NASA DC-8 during KORUS-AQ were supported by the Austrian Federal Ministry for Transport, Innovation and Technology (bmvit) through the Austrian Space Applications Programme (ASAP) of the Austrian Research Promotion Agency (FFG).

Competing interests

The authors have no competing interests to declare.

Author contributions

- Contributed to conception and design: JRS and JHC
- Contributed to acquisition of data: all authors
- Contributed to analysis and interpretation of data: JRS and JHC
- Drafted, revised, and approved of manuscript for submission: JRS and JHC

References

Chameides, WL, Xingsheng, L, Xiaoyan, T, Xiuji, Z, Luo, C, Kiang, CS, St. John, J, Saylor, RD, Liu, SC, Lam, KS and **Wang, T.** 1999. Is ozone pollution affecting crop yields in China? *Geophysical Research Letters* **26**(7): 867–870. DOI: https://doi.org/10.1029/1999GL900068

Chang, KL, Petropavlovskikh, I, Cooper, OR, Schultz, MG and **Wang, T.** 2017. Regional trend analysis of surface ozone observations from monitoring networks in eastern North America, Europe and East Asia. *Elem Sci Anth* **5**: 50. DOI: https://doi.org/10.1525/elementa.243

Choi, Y and **Souri, AH.** 2015. Chemical condition and surface ozone in large cities of Texas during the last decade: Observational evidence from OMI, CAMS, and model analysis. *Remote Sensing of Environment* **168**(2): 90–101. DOI: https://doi.org/10.1016/j.rse.2015.06.026

Colman, J, Swanson, AL, Meinardi, S, Sive, BC, Blake, DR and **Rowland, FS.** 2001. Description of the analysis of a wide range of volatile organic compounds in whole air samples collected during PEM-Tropics A and B. *Analytical Chemistry* **73**: 3723–3731. DOI: https://doi.org/10.1021/ac010027g

Crawford, J, Davis, D, Olson, J, Chen, G, Liu, S, Gregory, G, Barrick, J, Sachse, G, Sandholm, S, Heikes, B and **Singh, H.** 1999. Assessment of upper tropospheric HO_x sources over the tropical Pacific based on NASA GTE/PEM data: Net

effect on HO_x and other photochemical parameters. *Journal of Geophysical Research: Atmospheres* **104**(D13): 16255–16273. DOI: https://doi.org/10.1029/1999JD900106

Crounse, JD, McKinney, KA, Kwan, AJ and **Wennberg, PO.** 2006. Measurement of gas-phase hydroperoxides by chemical ionization mass spectrometry. *Analytical chemistry* **78**(19): 6726–6732. DOI: https://doi.org/10.1021/ac0604235

Diskin, GS, Podolske, JR, Sachse, GW and **Slate, TA.** 2002. *Open-Path Airborne Tunable Diode Laser Hygrometer*, 196–204. s.l: s.n. DOI: https://doi.org/10.1117/12.453736

Duncan, BN, Yoshida, Y, Olson, JR, Sillman, S, Martin, RV, Lamsal, L, Hu, Y, Pickering, KE, Retscher, C, Allen, DJ and **Crawford, JH.** 2010. Application of OMI observations to a space-based indicator of NO_x and VOC controls on surface ozone formation. *Atmospheric Environment* **44**(18): 2213–2223. DOI: https://doi.org/10.1016/j.atmosenv.2010.03.010

Edwards, PM, Young, CJ, Aikin, K, DeGouw, J, Dubé, WP, Geiger, F, Gilman, J, Helmig, D, Holloway, JS, Kercher, J and **Lerner, B.** 2013. Ozone photochemistry in an oil and natural gas extraction region during winter: simulations of a snow-free season in the Uintah Basin, Utah. *Atmospheric Chemistry and Physics* **13**(17): 8955–8971. DOI: https://doi.org/10.5194/acp-13-8955-2013

Fleming, ZL, Doherty, RM, Von Schneidemesser, E, Malley, C, Cooper, OR, Pinto, JP, Colette, A, Xu, X, Simpson, D, Schultz, MG and **Lefohn, AS.** 2018. Tropospheric Ozone Assessment Report: Present-day ozone distribution and trends relevant to human health. *Elementa: Science of the Anthropocene*. DOI: https://doi.org/10.1525/elementa.273

Fried, A, Cantrell, C, Olson, J, Crawford, JH, Weibring, P, Walega, J, Richter, D, Junkermann, W, Volkamer, R, Sinreich, R and **Heikes, BG.** 2011. Detailed comparisons of airborne formaldehyde measurements with box models during the 2006 INTEX-B and MILAGRO campaigns: potential evidence for significant impacts of unmeasured and multi-generation volatile organic carbon compounds. *Atmospheric Chemistry and Physics* **11**(22): 11867–11894. DOI: https://doi.org/10.5194/acp-11-11867-2011

Ghim, YS and **Chang, Y-S.** 2000. Characteristics of ground-level ozone distributions in Korea for the period of 1990–1995. *Journal of Geophysical Research: Atmospheres* **105**(D7): 8877–8890. DOI: https://doi.org/10.1029/1999JD901179

Goldberg, DL, Vinciguerra, TP, Anderson, DC, Hembeck, L, Canty, TP, Ehrman, SH, Martins, DK, Stauffer, RM, Thompson, AM, Salawitch, RJ and **Dickerson, RR.** 2016. CAMx ozone source attribution in the eastern United States using guidance from observations during DISCOVER-AQ Maryland. *Geophysical research letters* **43**(5): 2249–2258. DOI: https://doi.org/10.1002/2015GL067332

Haagen-Smit, AJ, Darley, EF, Zaitlin, M, Hull, H and **Noble, W.** 1952. Investigation on injury to plants from air pollution in the Los Angeles area. *Plant Physiology* **27**(1): 18. DOI: https://doi.org/10.1104/pp.27.1.18

Heck, WW, Taylor, OC, Adams, R, Bingham, G, Miller, J, Preston, E and **Weinstein, L.** 1982. Assessment of crop loss from ozone. *Journal of the Air Pollution Control Association* **32**(4): 353–361. DOI: https://doi.org/10.1080/00022470.1982.10465408

Jerrett, M, Burnett, RT, Pope III, CA, Ito, K, Thurston, G, Krewski, D, Shi, Y, Calle, E and **Thun, M.** 2009. Long-term ozone exposure and mortality. *New England Journal of Medicine* **360**(11): 1085–1095. DOI: https://doi.org/10.1056/NEJMoa0803894

Jo, WK and **Nam, CW.** 1999. Characteristics of urban ground-level ozone in korea. *Journal of the Air and Waste Management Association* **49**(12): 1425–1433. DOI: https://doi.org/10.1080/10473289.1999.10463979

Jo, WK, Yoon, IH and **Nam, CW.** 2000. Analysis of air pollution in two major Korean cities: Trends, seasonal variations, daily 1-hour maximum versus other hour-based concentrations, and standard exceedances. *Environmental Pollution* **110**(1): 11–18. DOI: https://doi.org/10.1016/S0269-7491(99)00284-5

Jung, HC, Moon, BK and **Wie, J.** 2018. Seasonal changes in surface ozone over South Korea. *Heliyon* **4**(1): e00515. DOI: https://doi.org/10.1016/j.heliyon.2018.e00515

Kim, JH, Lee, HJ and **Lee, SH.** 2006. The characteristics of tropospheric ozone seasonality observed from ozone soundings at Pohang, Korea. *Environmental Monitoring and Assessment* **118**(1–3): 1–12. DOI: https://doi.org/10.1007/s10661-006-0772-7

Kim, S, Jeong, D, Sanchez, D, Wang, M, Seco, R, Blake, D, Meinardi, S, Barletta, B, Hughes, S, Jung, J and **Kim, D.** 2018. The controlling factors of photochemical ozone production in Seoul, South Korea. *Aerosol and Air Quality Research* **18**(9): 2253–2261. DOI: https://doi.org/10.4209/aaqr.2017.11.0452

Kim, SY, Lee, JT, Hong, YC, Ahn, KJ and **Kim, H.** 2004. Determining the threshold effect of ozone on daily mortality: an analysis of ozone and mortality in Seoul, Korea, 1995–1999. *Environmental research* **94**(2): 113–119. DOI: https://doi.org/10.1016/j.envres.2003.09.006

Kleinman, LI. 1994. Low and high NO_x tropospheric photochemistry. *Journal of Geophysical Research* **99**(94): 831–838. DOI: https://doi.org/10.1029/94JD01028

Kleinman, LI, Daum, PH, Imre, D, Lee, YN, Nunnermacker, LJ, Springston, SR,

Weinstein-Lloyd, J and **Rudolph, J.** 2002. Ozone production rate and hydrocarbon reactivity in 5 urban areas: A cause of high ozone concentration in Houston. *Geophysical Research Letters* **29**(10): 105–1. DOI: https://doi.org/10.1029/2001GL014569

Kleinman, LI, Daum, PH, Lee, YN, Nunnermacker, LJ, Springston, SR, Weinstein-Lloyd, J and **Rudolph, J.** 2001. Sensitivity of ozone production rate to ozone precursors. *Geophysical Research Letters* **28**(15): 2903–2906. DOI: https://doi.org/10.1029/2000GL012597

Lurmann, FW, Lloyd, AC and **Atkinson, R.** 1986. A Chemical Mechanism for Use in Long-Range Transport/Acid Deposition Computer Modeling. *Journal of Geophysical Research* **91**(10): 905–10,936. DOI: https://doi.org/10.1029/JD091iD10p10905

Mao, J, Ren, X, Chen, S, Brune, WH, Chen, Z, Martinez, M, Harder, H, Lefer, B, Rappenglueck, B, Flynn, J and **Leuchner, M.** 2010. Atmospheric oxidation capacity in the summer of Houston 2006: Comparison with summer measurements in other metropolitan studies. *Atmospheric Environment* **44**(33): 4107–4115. DOI: https://doi.org/10.1016/j.atmosenv.2009.01.013

Mazzuca, GM, Ren, X, Loughner, CP, Estes, M, Crawford, JH, Pickering, KE, Weinheimer, AJ and **Dickerson, RR.** 2016. Ozone production and its sensitivity to NO_x and VOCs: results from the DISCOVER-AQ field experiment, Houston 2013. DOI: https://doi.org/10.5194/acp-2016-215

Müller, M, Mikoviny, T, Feil, S, Haidacher, S, Hanel, G, Hartungen, E, Jordan, A, Märk, L, Mutschlechner, P, Schottkowsky, R and **Sulzer, P.** 2014. A compact PTR-ToF-MS instrument for airborne measurements of volatile organic compounds at high spatiotemporal resolution. *Atmospheric Measurement Techniques* **7**(11): 3763–3772. DOI: https://doi.org/10.5194/amt-7-3763-2014

Oak, YJ, Park, RJ, Schroeder, JR, Crawford, JH, Blake, DR, Weinheimer, AJ, Woo, JH, Kim, SW, Yeo, H, Fried, A, Wisthaler, A and **Brune, WH.** 2019. Evaluation of simulated O_3 production efficiency during the KORUS-AQ campaign: Implications for anthropogenic NO_x emissions in Korea. *Elementa: Science of the Anthropocene*. DOI: https://doi.org/10.1525/elementa.394

Olson, JR, Crawford, JH, Chen, G, Brune, WH, Faloona, IC, Tan, D, Harder, H and **Martinez, M.** 2006. A reevaluation of airborne HO_x observations from NASA field campaigns. *Journal of Geophysical Research: Atmospheres* **111**(D10). DOI: https://doi.org/10.1029/2005JD006617

Olson, JR, Crawford, JH, Davis, DD, Chen, G, Avery, MA, Barrick, JDW, Sachse, GW, Vay, SA, Sandholm, ST, Tan, D and **Brune, WH.** 2001. Seasonal differences in the photochemistry of the South Pacific: A comparison of observations and model results from PEM-Tropics A and B. *Journal of Geophysical Research: Atmospheres* **106**(D23): 32749–32766. DOI: https://doi.org/10.1029/2001JD900077

Parrish, DD, Ryerson, TB, Mellqvist, J, Johansson, J, Fried, A, Richter, D, Walega, JG, Washenfelder, RD, De Gouw, JA, Peischl, J and **Aikin, KC.** 2012. Primary and secondary sources of formaldehyde in urban atmospheres: Houston Texas region. *Atmospheric Chemistry and Physics* **12**(7): 3273–3288. DOI: https://doi.org/10.5194/acp-12-3273-2012

Ren, X, Van Duin, D, Cazorla, M, Chen, S, Mao, J, Zhang, L, Brune, WH, Flynn, JH, Grossberg, N, Lefer, BL and **Rappenglück, B.** 2013. Atmospheric oxidation chemistry and ozone production: Results from SHARP 2009 in Houston, Texas. *Journal of Geophysical Research: Atmospheres* **118**(11): 5770–5780. DOI: https://doi.org/10.1002/jgrd.50342

Richter, D, Weibring, P, Walega, JG, Fried, A, Spuler, SM and **Taubman, MS.** 2015. Compact highly sensitive multi-species airborne mid-IR spectrometer. *Applied Physics B* **119**(1): 119–131. DOI: https://doi.org/10.1007/s00340-015-6038-8

Sachse, GW, Collins Jr, JE, Hill, GF, Wade, LO, Burney, LG and **Ritter, JA.** 1991, May. Airborne tunable diode laser sensor for high-precision concentration and flux measurements of carbon monoxide and methane. In *Measurement of atmospheric gases* **1433**: 157–166. International Society for Optics and Photonics. DOI: https://doi.org/10.1117/12.46162

Schroeder, JR, Crawford, JH, Fried, A, Walega, J, Weinheimer, A, Wisthaler, A, Müller, M, Mikoviny, T, Chen, G, Shook, M and **Blake, DR.** 2016. Formaldehyde column density measurements as a suitable pathway to estimate near-surface ozone tendencies from space. *Journal of Geophysical Research: Atmospheres* **121**(21): 13–088. DOI: https://doi.org/10.1002/2016JD025419

Schroeder, JR, Crawford, JH, Fried, A, Walega, J, Weinheimer, A, Wisthaler, A, Müller, M, Mikoviny, T, Chen, G, Shook, M and **Blake, DR.** 2017. New insights into the column CH2O/NO2 ratio as an indicator of near-surface ozone sensitivity. *Journal of Geophysical Research: Atmospheres* **122**(16): 8885–8907. DOI: https://doi.org/10.1002/2017JD026781

Seo, J, Park, DSR, Kim, JY, Youn, D, Lim, YB and **Kim, Y.** 2018. Effects of meteorology and emissions on urban air quality: a quantitative statistical approach to long-term records (1999–2016) in Seoul, South Korea. *Atmospheric Chemistry and Physics* **18**(21): 16121–16137. DOI: https://doi.org/10.5194/acp-18-16121-2018

Shetter, RE and **Müller, M.** 1999. Photolysis frequency measurements using actinic flux spectroradiometry during the PEM-Tropics mission: Instrumentation description and some results. *Journal of Geophysical Research: Atmospheres* **104**(D5): 5647–5661. DOI: https://doi.org/10.1029/98JD01381

Sillman, S. 1995. The use of NO_y, $H2O_2$, and HNO_3 as indicators for ozone-NO_x -hydrocarbon sensitivity in urban locations. *Journal of Geophysical Research: Atmospheres* **100**(D7): 14175–14188. DOI: https://doi.org/10.1029/94JD02953

Sillman, S. 2003. O_3-NO_x-VOC sensitivity and NO_x-VOC indicators in Paris: Results from models and Atmospheric Pollution Over the Paris Area (ESQUIF) measurements. *Journal of Geophysical Research* **108**(D17): 8563. DOI: https://doi.org/10.1029/2002JD001561

Sillman, S and **He, D.** 2002. Some theoretical results concerning O_3-NO_x-VOC chemistry and NO_x-VOC indicators. *Journal of Geophysical Research* **107**(D22): 4659. DOI: https://doi.org/10.1029/2001JD001123

Sillman, S, He, D, Pippin, MR, Daum, PH, Imre, DG, Kleinman, LI, Lee, JH and **Weinstein-Lloyd, J.** 1998. Model correlations for ozone, reactive nitrogen, and peroxides for Nashville in comparison with measurements: Implications for O_3-NO_x-hydrocarbon chemistry. *Journal of Geophysical Research: Atmospheres* **103**(D17): 22629–22644. DOI: https://doi.org/10.1029/98JD00349

Sillman, S, Logan, J and **Wofsy, S.** 1990. The sensitivity of ozone to nitrogen oxides and hydrocarbons in regional ozone episodes. *Journal of Geophysical Research* **95**: 1837–1851. DOI: https://doi.org/10.1029/JD095iD02p01837

Slusher, DL, Huey, LG, Tanner, DJ, Flocke, FM and **Roberts, JM.** 2004. A thermal dissociation–chemical ionization mass spectrometry (TD-CIMS) technique for the simultaneous measurement of peroxyacyl nitrates and dinitrogen pentoxide. *Journal of Geophysical Research: Atmospheres* **109**(D19). DOI: https://doi.org/10.1029/2004JD004670

Smith, DF, McIver, CD and **Kleindienst, TE.** 1998. Primary Product Distribution from the Reaction of Hydroxyl Radical with Toluene at ppb NO_x Mixing Ratios. *Journal of Atmospheric Chemistry* **30**(2): 209–228. DOI: https://doi.org/10.1023/A:1005980301720

Thornton, JA, Wooldridge, PJ, Cohen, RC, Martinez, M, Harder, H, Brune, WH, Williams, EJ, Roberts, JM, Fehsenfeld, FC, Hall, SR and **Shetter, RE.** 2002. Ozone production rates as a function of NO_x abundances and HO_x production rates in the Nashville urban plume. *Journal of Geophysical Research: Atmospheres* **107**(D12): ACH-7. DOI: https://doi.org/10.1029/2001JD000932

Tuazon, EC, Atkinson, R, Mac Leod, H, Biermann, HW, Winer, AM, Carter, WP and **Pitts, JN.** 1984. Yields of glyoxal and methylglyoxal from the nitrogen oxide (NO_x)-air photooxidations of toluene and m-and p-xylene. *Environmental science & technology* **18**(12): 981–984. DOI: https://doi.org/10.1021/es00130a017

Valin, LC, Fiore, AM, Chance, K and **González Abad, G.** 2015. The role of OH production in interpreting the variability of CH_2O columns in the southeast U.S. *Journal of Geophysical Research: Atmospheres* **121**: 3510–3532. DOI: https://doi.org/10.1002/2015JD024012

Weibring, P, Richter, D, Walega, JG, Rippe, L and **Fried, A.** 2010. Difference frequency generation spectrometer for simultaneous multispecies detection. *Optics express* **18**(26): 27670–27681. DOI: https://doi.org/10.1364/OE.18.027670

Weinheimer, AJ, Walega, JG, Ridley, BA, Gary, BL, Blake, DR, Blake, NJ, Rowland, FS, Sachse, GW, Anderson, BE and **Collins, JE.** 1994. Meridional distributions of NO_x, NO_y, and other species in the lower stratosphere and upper troposphere during AASE II. *Geophysical research letters* **21**(23): 2583–2586. DOI: https://doi.org/10.1029/94GL01897

Wert, BP. 2003. Signatures of terminal alkene oxidation in airborne formaldehyde measurements during TexAQS 2000. *Journal of Geophysical Research* **108**(D3): 4104. DOI: https://doi.org/10.1029/2002JD002502

Wolfe, GM, Kaiser, J, Hanisco, TF, Keutsch, FN, de Gouw, JA, Gilman, JB, Graus, M, Hatch, CD, Holloway, J, Horowitz, LW and **Lee, BH.** 2016. Formaldehyde production from isoprene oxidation across NO_x regimes. *Atmospheric chemistry and physics* **16**(4): 2597–2610. DOI: https://doi.org/10.5194/acp-16-2597-2016

Zhang, Y, Wang, Y, Chen, G, Smeltzer, C, Crawford, J, Olson, J, Szykman, J, Weinheimer, AJ, Knapp, DJ, Montzka, DD and **Wisthaler, A.** 2016. Large vertical gradient of reactive nitrogen oxides in the boundary layer: Modeling analysis of DISCOVER-AQ 2011 observations. *Journal of Geophysical Research: Atmospheres* **121**(4): 1922–1934. DOI: https://doi.org/10.1002/2015JD024203

Zhou, W, Cohan, DS and **Napelenok, SL.** 2013. Reconciling NO_x emissions reductions and ozone trends in the U.S., 2002–2006. *Atmospheric Environment* **70**(x): 236–244. DOI: https://doi.org/10.1016/j.atmosenv.2012.12.038

How to cite this article: Schroeder, JR, Crawford, JH, Ahn, J-Y, Chang, L, Fried, A, Walega, J, Weinheimer, A, Montzka, DD, Hall, SR, Ullmann, K, Wisthaler, A, Mikoviny, T, Chen, G, Blake, DR, Blake, NJ, Hughes, SC, Meinardi, S, Diskin, G, Digangi, JP, Choi, Y, Pusede, SE, Huey, LG, Tanner, DJ, Kim, M and Wennberg, P. 2020. Observation-based modeling of ozone chemistry in the Seoul metropolitan area during the Korea-United States Air Quality Study (KORUS-AQ). *Elem Sci Anth,* 8: 3. DOI: https://doi.org/10.1525/elementa.400

Domain Editor-in-Chief: Detlev Helmig, Institute of Alpine and Arctic Research, University of Colorado Boulder, US

Associate Editor: Jochen Stutz, Atmospheric and Oceanic Sciences, University of California Los Angeles, US

Knowledge Domain: Atmospheric Science

Part of an *Elementa* Special Feature: KORUS-AQ

Submitted: 03 May 2019 **Accepted:** 16 November 2019 **Published:** 13 January 2020

ELEMENTA Science of the Anthropocene

Elem Sci Anth is a peer-reviewed open access journal published by University of California Press.

OPEN ACCESS